https://doi.org/10.5194/essd-2021-71
Preprint. Discussion started: 21 April 2021

Open Access Earth System Science Data Discussions

Catchment attributes and meteorology for large sample study in contiguous China

Zhen Hao[2], Jin Jin[1,2], Runliang Xia[2], Shimin Tian[2], Wushuang Yang[2], Qixing Liu[2], Min Zhu[2], Tao Ma[2], Chengran Jing[2]

[1]School of Computer Science, Northwestern Polytechnical University, Xi'an, China, 710072
[2]Yellow River Institute of Hydraulic Research, Zhengzhou, China, 450003

Correspondence to: Jin Jin (jinjinhao@21cn.com)

Abstract.

We introduce the first large-scale catchment attributes and meteorological time series dataset of contiguous China. To develop the dataset, we compiled diverse data sources to generate basin-oriented features describing the catchment characteristics related to hydrological processes. The proposed dataset consists of catchment characteristics, including soil, land cover, climate, topography, geology, and 29-year meteorological time series (from 1990 to 2018). The meteorological variables include precipitation, temperature, evapotranspiration, wind speed, ground surface temperature, pressure, humidity and sunshine duration. We also derived a daily potential evapotranspiration time series based on a modified Penman's equation. The studied catchments are 4875 catchments within contiguous China derived from digital elevation models. We analysed and organised the spatial variations of catchment characteristics into a series of maps. Correlation analysis between attributes was conducted. Compared to the previously proposed datasets, we derived more catchment characteristics resulting in 125 attributes, providing a complete description of the catchments. Besides, we propose Normal-Camels-YR, a hydrological dataset covering 102 basins of the Yellow River basin with normalized streamflow observations. The proposed dataset provides numerous opportunities for comparative hydrological research, such as examining the difference in hydrological behaviours across different catchments and building general rainfall-runoff modelling frameworks for many catchments instead of limited to a few. The dataset is freely available via http://doi.org/10.5281/zenodo.4704017 for community use. We will open-source the complement code for generating the dataset such that the user can generate meteorological series and catchment attributes for any watershed within contiguous China.

1 Introduction

Studying a large set of catchments often provides insights that cannot be obtained when looking at a single or few catchments (Coron, Andreassian et al. 2012, Kollat, Reed et al. 2012, Newman, Clark et al. 2015, Lane, Coxon et al. 2019). The hydrologic cycle consists of many sub-processes, including evaporation from the ocean, raindrop, interception, surface runoff, infiltration, etc. Catchment attributes such as soil characteristics, land cover characteristics and climate indices influence the water movement and storage in these sub-processes such that hydrologic behaviours can vary across catchments (van Werkhoven, Wagener et al. 2008). The same hydrological model may not be applicable in another basin. However, by examining a large sample of catchments, it is possible for the hydrological model to learn the similarities and differences of hydrological behaviours across catchments. For example, prediction in ungauged basins is a challenging problem present in hydrology. The central challenge is how to extrapolate hydrologic information from gauged basins to ungauged ones. Solving the problem relies on understanding the similarities and differences between different catchments. However, regionally and temporally imbalanced observations bring a difficulty to the problem. For a hydrologic model to successfully simulate the ungauged areas, it must adapt itself to the different hydrologic behaviours present in different catchments. (Kratzert, Klotz et al. 2019) shows encoding catchment characteristics (e.g., soil characteristics, land cover, topography) into a data-driven model can teach model to behave differently responding the meteorological time series input based on different sets of static catchment attributes.

(Silberstein 2006, Shen, Laloy et al. 2018, Nevo, Anisimov et al. 2019) pointed out that large sample hydrological datasets are the foundation and key of many hydrological studies. The term big hydrologic data refers to all data influencing the water cycle, such as the meteorological variables, infiltration characteristics of the study area, land use or land cover types, physical and geological features of the study area, etc. Many studies cannot be carried out without large-scale hydrologic data (Coron, Andreassian et al. 2012, Singh, van Werkhoven et al. 2014, Berghuijs, Aalbers et al. 2017, Gudmundsson, Leonard et al. 2019, Tyralis, Papacharalampous et al. 2019). For hydrological research, basin-orientated large sample datasets are of great significance. For example, comparative hydrology (de Araújo and González Piedra 2009, Singh, Archfield et al. 2014) focus on understanding how hydrological processes interact with the ecosystem, in particular, how hydrologic behaviours change under changes in the surface and sub-surface of the earth to determine to what extent hydrological predictions can be transferred from one area to another. Large-sample catchment attributes dataset provide opportunities for research studying interrelationships among catchment attributes. (Seybold, Rothman et al. 2017) studied the correlations between river junction angle with geometric factors, downstream concavity, and aridity. (Oudin, Andréassian et al. 2008) investigates the link between land cover and mean annual streamflow based on 1508 basins representing a large hydroclimatic variety. (Voepel, Ruddell et al. 2011) examines how the interaction of climate and topography influences vegetation response.

Data-driven methods can best benefit from large-scale data. Data-driven approaches have shown great potential in various fields, transforming the applications in many industries (LeCun, Bengio et al. 2015). However, data-driven methods, especially the deep learning-based approaches, usually require high data volumes. Limited data will cause the over-fitting (Blumer, Ehrenfeucht et al. 1987, Abu-Mostafa, Magdon-Ismail et al. 2012) problem. Therefore, big hydrologic data is the fundamental support for the successful deployment of powerful data-driven strategies.

Traditional hydrological models have some long standing challenges, such as the inability to capture hydrological processes' mechanism complexity (Kollat, Reed et al. 2012), which is due to the structural limitations of the conceptual models. Data-driven methods are proposed to overcome some existing obstacles. Data-driven strategies open a new way for researchers to acquire knowledge transforming the research pattern from hypothesis-driven to data-driven. (Feng, Fang et al. 2020) proposed a flexible data integration fusing various types of observations to improve rainfall-runoff modelling. The research shows that combining different resources of data benefits predictions in regions with high autocorrelation in streamflow. (Wongso, Nateghi et al. 2020) developed a model predicting the state-level, per capita water uses in the United States, taking various geographic, climatic, and socioeconomic variables as input. The research also identified key factors associated with high water usage. (Mei, Maggioni et al. 2020) proposed a statistical framework for spatial downscaling to obtain hyper-resolution precipitation data. The results show improvements compared with the original product. (Brodeur, Herman et al. 2020) applied machine learning techniques, namely bootstrap aggregation and cross-validation, to reduce overfitting in reservoir control policy search. (Ni and Benson 2020) proposed an unsupervised machine learning method to differentiate flow regimes and identify capillary heterogeneity trapping, showing the promise of machine learning methods for analysing large datasets from coreflooding experiments. (Legasa and Gutiérrez 2020) propose to apply Bayesian Network for multisite precipitation occurrence generation. The proposed methodology shows improvements for existing methods.

World-wide data sharing has become a trend (Wickel, Lehner et al. 2007, Ceola, Arheimer et al. 2015, Blume, van Meerveld et al. 2018, Wang, Chen et al. 2020), and the amounts of hydrologic data available are ever-increasing. However, these data typically came from different providers and are compiled in various formats. For example, ASTGTM[1] provides a global digital elevation model; GliM (Hartmann and Moosdorf 2012) includes rock types data globally; MODIS provides data products (Knyazikhin 1999, Didan 2015, Myneni, Knyazikhin et al. 2015, Running, Mu et al. 2017, Sulla-Menashe and Friedl 2018) describing features of the land and the atmosphere derived from remote sensing observations; (Yamazaki, Ikeshima et al. 2019) provides a global flow direction map at three arc-second resolution; HydroBASINS (Lehner 2014) provides basin boundaries at different scales globally; and GDBD (Masutomi, Inui et al. 2009) provides basin boundaries with geographic attributes; GLHYMPS (Gleeson, Moosdorf et al. 2014) provides a global map of subsurface permeability and porosity; SoilGrids250m (Hengl, Mendes de Jesus et al. 2017) dataset provides global numeric soil properties. Local government agencies often hold meteorological data such as precipitation and evaporation, and the amount of this data is also growing, however, data transparency has still been a problem (Viglione, Borga et al. 2010). The data mentioned above are rarely spatially aggregated to the catchment-scale, making it difficult for researchers to use these data. Properly pre-processed and formatted datasets on a large scale are of great importance for the hydrology research. Searching for appropriate data sources, pre-processing, and formatting often consumes a lot of researchers' time. In some cases, individual research groups either do not know where to obtain the appropriate data or cannot properly process the data to receive the desired format.

In summary, both data-driven and traditional hydrological research need diverse hydrologic datasets to learn the generalisation capability from one area to another. For a model to adapt to various behaviours in different catchments, the dataset must be

[1] https://asterweb.jpl.nasa.gov/gdem.asp

large enough to represent the complex heterogeneity presented in the natural hydrologic system. Although data sharing is being advocated in the community, it is usually difficult for the public to obtain certain data such as meteorological data and streamflow observations, either because there are not enough observations or because there are no open access permissions.

Recently, there are efforts (Addor, Newman et al. 2017, Alvarez-Garreton, Mendoza et al. 2018, Chagas, Chaffe et al. 2020, Coxon, Addor et al. 2020) compiling different types of data sources to form large scale hydrological datasets. These four collected datasets cover the continental United States, Chile, Brazil, and Great Britain. (Addor, Do et al. 2020) reviewed these datasets and discussed the guidelines for producing large-sample hydrological datasets and the limitations of the currently proposed datasets. The CAMELS dataset has been used to support a lot of research. Based on CAMELS, (Kratzert, Klotz et al. 2018) built a Long Short-Term Memory (LSTM) network for rainfall-runoff modelling, showing that one model can predict the discharge for a variety of catchments. (Knoben, Freer et al. 2019) compared metrics used in hydrology based on simulations on many basins. (Tyralis, Papacharalampous et al. 2019) studied the relationship between the shape parameter and basin attributes based on the sizeable basin-oriented dataset.

However, there is no large-scale compilation of hydrological datasets in contiguous China. An alternative is on a global scale, the HydroATLAS (Linke, Lehner et al. 2019) dataset. However, since it is on a world-wide scale, compared with other datasets constructed for regions, the dataset lacks many attributes and is not built according to the CAMELS standards. Besides, the climatic data is not up to date (1950-2000), and the derivation of climatic data lacks ground surface observations inputs, such that the data quality is not guaranteed.

Therefore, researchers still need to do repetitive works to compile data from different sources such as obtaining historical meteorological data (temperature, rainfall, evapotranspiration) of a catchment in contiguous China. Inspired by (Addor, Newman et al. 2017), in this paper, we present a catchment scale hydrologic dataset compiling a wide variety of hydrological data, including basin topography, climate indices, land cover characteristics, soil characteristics and geological characteristics covering contiguous China.

The proposed dataset is the first dataset providing catchments meteorological time series and catchments attributes of contiguous China. We compiled and named the dataset following most standards of the previously proposed datasets. Unlike CAMELS and CAMELS-CL, catchments in the proposed dataset are not selective. Instead, the dataset consists of all generated basins from the Digital Elevation Model (DEM), based on the Global Drainage Basin Dataset (Masutomi, Inui et al. 2009). The GDBD is derived at high-resolution (100m-1km) and has a good geographic agreement with existing global drainage basin data in China[2]. Besides, an essential feature of the proposed dataset is that it provides a complete description of the catchment, rather than an abstraction. For example, both CAMELS and CAMELS-CL only report the most frequent and second most frequent catchment land cover and lithology types. Instead, the proposed dataset calculates the proportion of each land cover and lithology type for each catchment to serve data-driven research better. We also introduced many more climate characteristics and soil characteristics to support more diverse potential research.

Researchers from different places can use the proposed dataset in conjunction with their streamflow data, simplifying organising and compiling various data resources, which is usually repetitive work. The proposed dataset is undoubtedly the most comprehensive catchment attributes and meteorological time series dataset in contiguous China and is suitable for multi-purpose data-driven research. The dataset consists of basin boundaries in the shapefile format, computed catchment attributes of climate, land cover, soil, topography and lithology and 29-year meteorological time series. Table 1 compares the number of static attributes between CAMELS, CAMELS-BR, and the proposed dataset.

The paper is organized as follows: Section 2 describes the study area. Section 3-7 describes the five classes of the computed catchment attributes. In section 3-7, each unit follows the same structure: first introduce the meaning and significance of each added feature and data source used, then describe the variables' spatial variability if necessary. Section 8 describes the proposed catchment-scale meteorological forcing time series. Section 9 introduce the Normal-Camels-YR dataset, which provides normalized streamflow measurements for 102 catchments of Yellow River. Section 10 describes the code and data availability. Section 11 presents the concluding remark.

In summary, our contributions are as follows:

(1) The proposed dataset is the first large-scale dataset containing catchment-scale meteorological time series of contiguous China, which is the basis for many hydrological studies.
(2) We present the first basin-oriented static attributes dataset in contiguous China.
(3) We introduce several new catchment characteristics providing a complete description of the catchment compared with the previously proposed datasets such that the proposed dataset is prepared for potential hydrological studies.
(4) We offer a self-contained dataset covering 102 basins of the Yellow River basin with normalized runoff observation supporting many potential studies.

[2] In this study, gauge streamflow measurements are not available in areas other than the Yellow River such that it is infeasible to specify a gauge location for generating the basin boundary for most of the areas. Streamflow measurements have strict redistribution policy; however, local research institutions have their streamflow measurements for hydrological research, the proposed dataset can used in conjunction with the streamflow data of researchers in various places.

https://doi.org/10.5194/essd-2021-71
Preprint. Discussion started: 21 April 2021

(5) We will open-source the code for generating the dataset such that the user can generate a dataset for any watershed within contiguous China.

Table 1 Number of computed attributes in CAMELS, CAMELS-BR and the proposed dataset.

Attribute class	CAMELS(A17)	CAMELS-BR	Ours
Location and topography	9	11	12
Geology	7	7	18
Soil	11	6	54
Land cover	8	11	22
Climatic indices	11	13	17
Human intervention indices	not computed	4	2
Total	46	52	125

Table 2 Summary of basin daily discharge and forcing data in CAMELS, CAMELS-BR and the proposed dataset.

Forcing data class	CAMELS	CAMELS-BR	Ours
Temperature	available	available	available
Precipitation	available	available	available
Solar radiation	available	**not available**	available
Day length	available	**not available**	**not available**
Sunshine hours	**not available**	**not available**	available
Humidity	available	**not available**	available
Snow water equivalent	available	**not available**	**not available**
Wind velocity	**not available**	**not available**	available
Ground surface pressure	available	**not available**	available
Observed evaporation	**not available**	available	available
Potential evapotranspiration	**not available**	available	available
Streamflow	available	available	partially available (see Section 9)

2 Study area

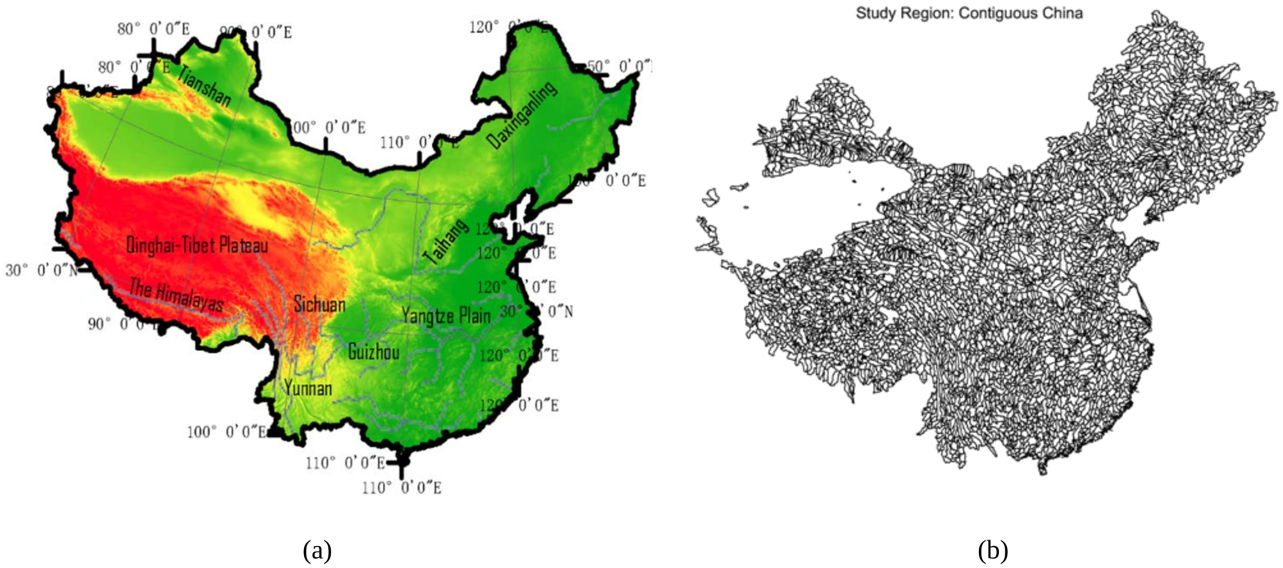

Figure 1. Overview of the study area. The study area covers a wide range of latitude and longitude, from 18.2° N to 52.3° N, and from 76.0° E to 134.3° E. (a) The main geographical features map of contiguous China. China is mountainous; mountains and hills occupy two-thirds of the area. (b) The distribution map of the delimited catchments based on the ASTER DEM, the catchments studied are all catchment areas delimited from the DEM, covering contiguous China, with 4875 catchments, most of which are 2000 to 5000 square kilometres.

The study area corresponds to contiguous China, with diverse climate and terrain characteristics, spanning from 18.2° N to 52.3° N and 76.0° E to 134.3° E. Mountains, plateaus, and hills account for about two-thirds of areas of contiguous China, and the remaining are basins and plains. China’s topography is like a three-level ladder, high in the west and low in the east. The Qinghai-Tibet Plateau, the highest plateau globally, located in the west of contiguous China, with a mean elevation of over 4000 meters, is the first step of China’s topography. The Xinjiang region, the Loess Plateau, the Sichuan Basin, and the Yunnan-Guizhou Plateau to the north and east are the second step of China’s topography. The mean sea level here is between 1000 to 2000 meters. Plains and hills dominate the east of the Daxinganling-Taihang Mountain to the coastline, the third step of contiguous China. The elevation of this step descends to 500-1,000 meters.

In contiguous China, precipitation and temperature vary significantly in different places, forming a diverse climate environment. According to the Köppen Climate Classification System, from northwest to southeast, China’s climate gradually evolves from Cold desert (BW_k) climate, Tundra (ET) climate, Warm and temperate continental (D_{fa} and D_{wb}) climate to Humid subtropical (C_{wa}) climate and Warm oceanic (C_{fa}) climate. From the perspective of temperature zones, there are tropical, subtropical, warm temperate, medium temperate, cold temperate and Qinghai-Tibet Plateau regions, and there are humid regions, semi-humid regions, semiarid regions, and arid regions from the perspective of wet and dry zones. Moreover, the same temperature zone can contain different dry and wet zones. Therefore, there will be differences in heat and wetness in the same climate type. The complexity of the terrain makes the climate even more complex and diverse. Besides, China has a wide range of regions affected by the alternating winter and summer monsoons. Compared with other parts of the world at the same latitude, these areas have low winter temperatures, high summer temperatures, significant annual temperature differences, and concentrated precipitation in summer. The cold and dry winter monsoon occurs in Asia's interior, far away from the ocean. Under its influence, winter rainfall in most parts of China is low, accompanied by low temperature. The summer monsoon is warm and humid, coming from the Pacific Ocean and the Indian Ocean. Under its influence, precipitation generally increases.

Table 3 Summary table of catchment attributes available in the proposed dataset

Attribute class	**Attribute name**	**Description**	**Unit**	**Data source**
Climate indices (computed for 1 Oct 1990 to 30 Sep 2018)	pet_mean	mean daily pet (Penman–Monteith equation)	mm d^{-1}	(Subramanya 2013)
	evp_mean	mean daily evaporation (observations)	mm d^{-1}	SURF_CLI_CHN_MUL_DAY[3]
	gst_mean	mean daily ground surface temperature	°C	
	pre_mean	mean daily precipitation	mm d^{-1}	
	prs_mean	mean daily ground surface pressure	hPa	
	rhu_mean	mean daily relative humidity	-	
	ssd_mean	mean daily sunshine duration	h	
	tem_mean	mean daily temperature	°C	
	win_mean	mean daily wind speed	m s^{-1}	
	p_seasonality	seasonality and timing of precipitation (estimated using sine curves to represent the annual temperature and precipitation cycles, positive [negative] values indicate that precipitation peaks in summer [winter], values close to 0 indicate uniform precipitation throughout the year)	-	

[3] http://data.cma.cn/data/cdcdetail/dataCode/SURF_CLI_CHN_MUL_DAY.html

	high_prec_freq	frequency of high-precipitation days (⩾ 5 times mean daily precipitation)	d yr^{-1}	
	high_prec_dur	average duration of high-precipitation events (number of consecutive days ⩾ 5 times mean daily precipitation)	d	
	high_prec_timing	season during which most high-precipitation days (⩾ 5 times mean daily precipitation) occur	season	
	low_prec_freq	frequency of dry days (< 1mm d^{-1})	d yr^{-1}	
	low_prec_dur	average duration of dry periods (number of consecutive days < 1 mm d^{-1})	d	
	low_prec_timing	season during which most dry days (< 1 mm d^{-1}) occur	season	
	frac_snow_daily	fraction of precipitation falling as snow (for days colder than 0 °C)	-	
	p_seasonality	seasonality and timing of precipitation, positive [negative] values indicate that precipitation peaks in summer [winter], values close to 0 indicate uniform precipitation throughout the year	-	
Geological characteristics	geol_porosity	subsurface porosity	-	(Gleeson, Moosdorf et al. 2014)
	geol_permeability	subsurface permeability (log-10)	m^2	
	ig	fraction of the catchment area associated with ice and glaciers	-	(Hartmann and Moosdorf 2012)
	pa	fraction of the catchment area associated with acid plutonic rocks	-	
	sc	fraction of the catchment area associated with carbonate sedimentary rocks	-	

https://doi.org/10.5194/essd-2021-71
Preprint. Discussion started: 21 April 2021

su	fraction of the catchment area associated with unconsolidated sediments	-
sm	fraction of the catchment area associated with mixed sedimentary rocks	-
vi	fraction of the catchment area associated with intermediate volcanic rocks	-
mt	fraction of the catchment area associated with metamorphic	-
ss	fraction of the catchment area associated with siliciclastic sedimentary rocks	-
pi	fraction of the catchment area associated with intermediate plutonic rocks	-
va	fraction of the catchment area associated with acid volcanic rocks	-
wb	fraction of the catchment area associated with water bodies	-
pb	fraction of the catchment area associated with basic plutonic rocks	-
vb	fraction of the catchment area associated with basic volcanic rocks	-
nd	fraction of the catchment area associated with no data	-
py	fraction of the catchment area associated with pyroclastic	-
ev	fraction of the catchment area associated with evaporites	-

Land cover characteristics	lai_max	maximum monthly mean of the leaf area index (based on 12 monthly means)	-	(Myneni, Knyazikhin et al. 2015)
	lai_diff	difference between the maximum and minimum monthly mean of the leaf area index (based on 12 monthly means)	-	
	ndvi_mean	mean normalized difference vegetation index (NDVI)	-	(Didan 2015)
	root_depth_50	root depth (percentiles=50% extracted from a root depth distribution based on IGBP land cover)	m	Eq. 2 and Table 2 in (Zeng 2001)
	root_depth_99	root depth (percentiles=99% extracted from a root depth distribution based on IGBP land cover)	m	
	evergreen needleleaf tree	catchment area fraction covered by evergreen needleleaf tree	-	(Sulla-Menashe and Friedl 2018)
	evergreen broadleaf tree	catchment area fraction covered by evergreen broadleaf tree	-	
	deciduous needleleaf tree	catchment area fraction covered by deciduous needleleaf forests	-	
	deciduous broadleaf tree	catchment area fraction covered by deciduous broadleaf tree	-	
	mixed forest	catchment area fraction covered by mixed forest	-	
	closed shrubland	catchment area fraction covered by closed shrubland	-	
	open shrubland	catchment area fraction covered by open shrubland	-	
	woody savanna	catchment area fraction covered by woody savanna	-	

	savanna	catchment area fraction covered by savanna	-	
	grassland	catchment area fraction covered by grassland	-	
	permanent wetland	catchment area fraction covered by permanent wetland	-	
	cropland	catchment area fraction covered by cropland	-	
	urban and built-up land	catchment area fraction covered by urban and built-up land	-	
	cropland/natural vegetation	catchment area fraction covered by cropland/natural vegetation	-	
	snow and ice	catchment area fraction covered by snow and ice	-	
	barren	catchment area fraction covered by barren	-	
	water bodies	catchment area fraction covered by water bodies	-	
Topography, location, and Human intervention	basin_id	drainage basin identifiers	-	(Masutomi, Inui et al. 2009)
	pop	population	people	
	pop_dnsty	population density	people km^{-2}	
	lat	mean latitude	°N	
	lon	mean longitude	°E	
	elev	mean elevation	M	
	area	catchment area	km^2	
	slope	mean slope	m km^{-1}	(Horn 1981)
	length	The length of the mainstream measured from the basin outlet to the remotest point on the basin boundary. The mainstream is identified by starting from the basin	km	(Subramanya 2013)

		outlet and moving up the catchment.		
	form factor	catchment area / (catchment length)^2	-	
	shape factor	(catchment length)^2 / catchment area	-	
	compactness coefficient	perimeter of the catchment / perimeter of the circle whose area is that of the basin	-	
	circulatory ratio	catchment area / area of circle of catchment perimeter	-	
	elongation ratio	diameter of circle whose area is basin area / catchment length	-	
Soil	pdep	soil profile depth	cm	(Shangguan, Dai et al. 2013)
	clay	percentage of clay content of the soil material	%	
	sand	percentage of sand content of the soil material	%	
	por	porosity	cm^3 cm^{-3}	
	silt	percentage of silt content of the soil material	%	
	grav	rock fragment content	%	
	som	soil organic carbon content	%	
	log_k_s[4]	log-10 transformation of saturated hydraulic conductivity	cm d^{-1}	(Dai, Xin et al. 2019)
	theta_s[4]	saturated water content	cm^3 cm^{-3}	
	tksatu[4]	thermal conductivity of unfrozen saturated soils	W m^{-1} K^{-1}	
	bldfie[4]	bulk density	kg m^{-3}	

[4] The data source contains multi-layer soil data, soil characteristics for all layers are determined.

	cecsol[4]	cation-exchange capacity	cmol+ kg^{-1}	(Hengl, Mendes de Jesus et al. 2017)
	orcdrc[4]	organic carbon content	g kg^{-1}	
	phihox[4]	pH in H2O	10^{-1}	
	bdticm	depth to bedrock	cm	

3 Climate indices

Meteorological raw data was provided by the China Meteorological Data Network[3], released as the SURF_CLI_CHN_MUL_DAY (V3.0) dataset, which provides complete variable types and the longest period (1951-2018) of meteorological time series of China. The SURF_CLI_CHN_MUL_DAY product includes site observations of pressure, temperature, relative humidity, precipitation, evaporation, wind speed, sunshine duration, and ground surface temperature. The summary is presented in Table 4. The Inverse distance weighting method is used for interpolating the site observations. Climate indices are then obtained by taking the average of the catchment-scale extraction from the interpolated raster. To ensure data quality, we chose the latter 29-year record (from 1990 to 2018) to construct the dataset since sites' distribution was sparse in the early days (Fig. 2). We computed more climatic characteristics compared with other datasets (Table 2). These characteristics have critical potential effects on the hydrological processes; for example, wind speed can affect actual evapotranspiration. To be consistent with the CAMELS (Addor, Newman et al. 2017), we also determined all climatic attributes (Woods 2009) in the CAMELS dataset. The proposed dataset provides more meteorological variables and longer time series (1990-2018) than CAMELS and CAMELS-CL. A summary of the computed Climate indices is presented in Table 3. The national distribution of meteorological attributes of catchments is shown in Fig. 3.

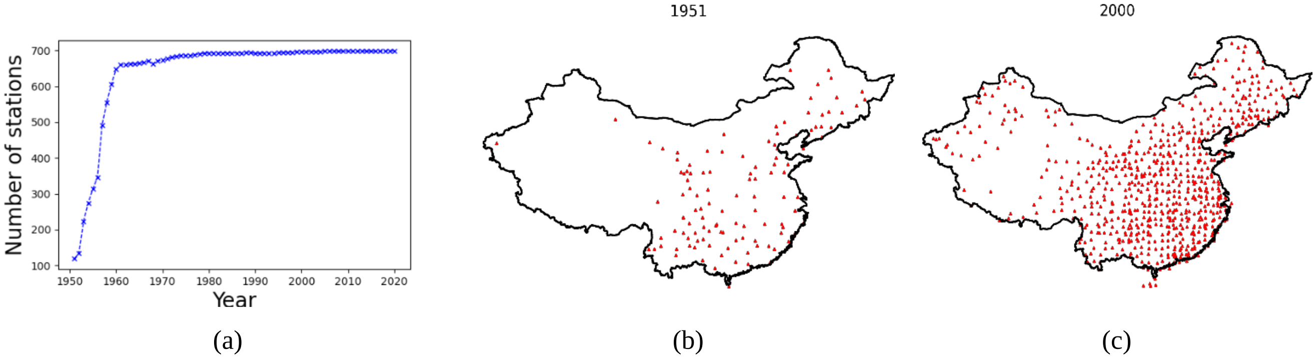

Figure 2. Overview of changes in the number and distribution of meteorological stations in China. (a) The number of meteorological stations varies with the year. There were only 119 stations in 1951. This number increased rapidly from 1951 to the early 1960s, and the number of stations remained stable after 2000. (b) Distribution map of China's meteorological stations in 1951. (c) Distribution map of China's meteorological stations in 2000.

https://doi.org/10.5194/essd-2021-71
Preprint. Discussion started: 21 April 2021

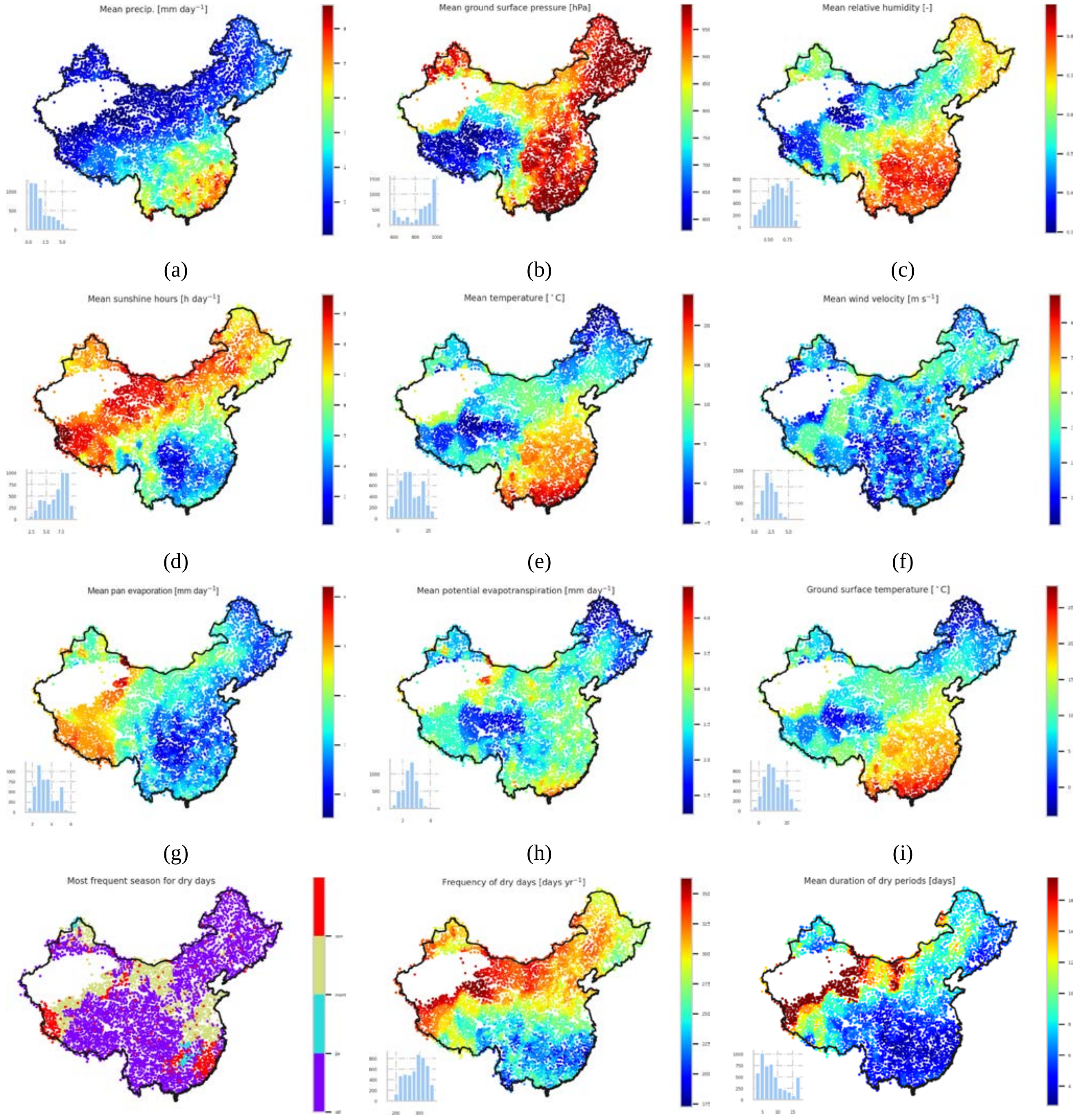
Mean precip. [mm day^{-1}]
Mean ground surface pressure [hPa]
Mean relative humidity [-]
Mean sunshine hours [h day^{-1}]
Mean temperature [$^\circ$C]
Mean wind velocity [m s^{-1}]
Mean pan evaporation [mm day^{-1}]
Mean potential evapotranspiration [mm day^{-1}]
Ground surface temperature [$^\circ$C]
Most frequent season for dry days
Frequency of dry days [days yr^{-1}]
Mean duration of dry periods [days]

(a) (b) (c)

(d) (e) (f)

(g) (h) (i)

(j) (k) (l)

https://doi.org/10.5194/essd-2021-71
Preprint. Discussion started: 21 April 2021

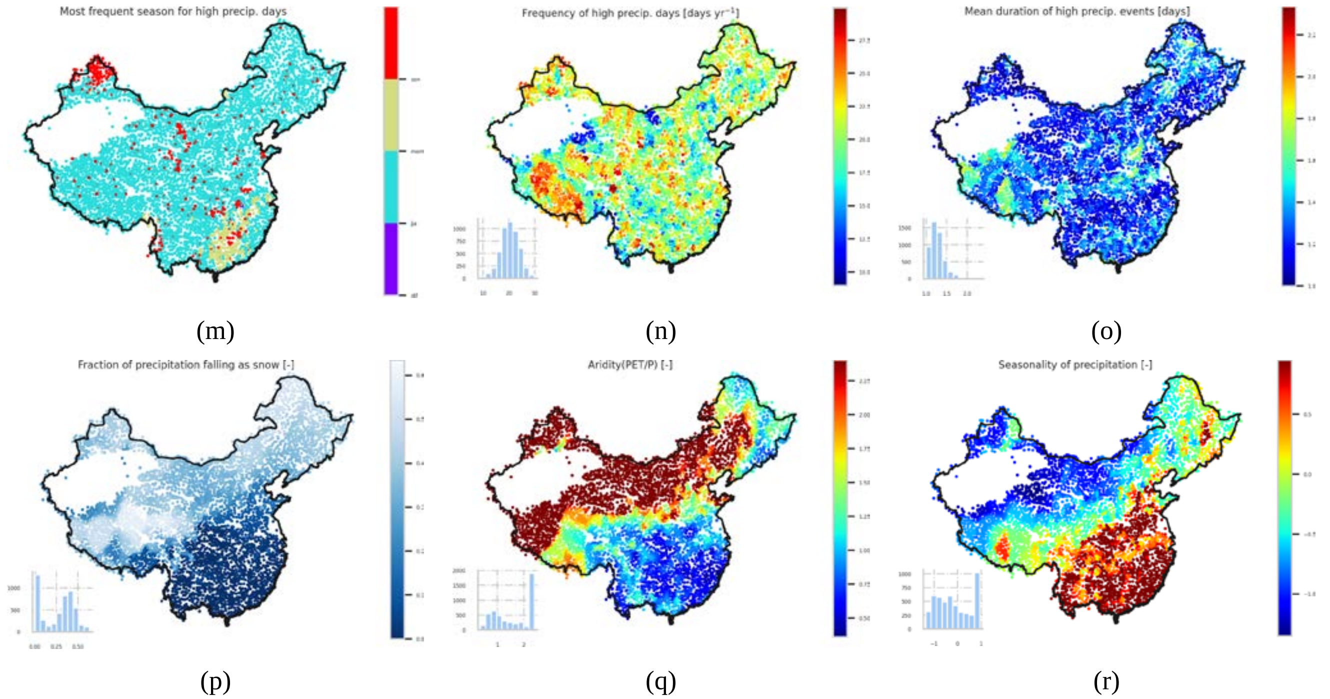
Most frequent season for high precip. days
Frequency of high precip. days [days yr⁻¹]
Mean duration of high precip. events [days]
Fraction of precipitation falling as snow [-]
Aridity(PET/P) [-]
Seasonality of precipitation [-]

(m) (n) (o)

(p) (q) (r)

Figure 3. Maps of climatic indices over contiguous China. The histograms and bar plots indicate the number of catchments (out of 4875) in each bin or category.

The instruments for measuring evaporation were updated from 2000 to 2005. Early observations can be multiplied by a correction coefficient to approximate the new tools. However, the coefficient varies across stations making the approach infeasible. To complement this, we calculated potential evapotranspiration (PET) based on a modified Penman's Equation (see Appendix) and other observed meteorological variables, providing a series of consistent evapotranspiration estimation.

The average daily precipitation in contiguous China is highest in the southeast and lowest in the northwest. It is also higher in the coastal areas than in the interior land. Ground surface pressure is positively correlated with elevation, the highest in the Qinghai-Tibet Plateau and the lowest in the Southeast Plain. The average relative humidity is generally positively correlated with precipitation; they are also higher in some forested areas, such as the Taihang Mountains and Daxingan Mountains. The Qinghai-Tibet Plateau has the lowest average temperature, and the southern coastal area has the highest. A distinctive feature of the distribution of wind speed is the high wind speed in mountainous areas. The highest wind speed occurs in the southeast coastal area (> 6 meters per second). Refer to Section 8 for a detailed description of the proposed catchment-scale meteorological time series dataset of contiguous China.

4 Geology

To describe the lithological characteristics of each catchment, we used the same two global datasets as CAMELS, Global Lithological Map (GLiM) (Hartmann and Moosdorf 2012) and GLobal HYdrogeology MaPS (GLHYMPS) (Gleeson, Moosdorf et al. 2014). Figure 4 presents the results.

GLiM provides a high resolution global lithological map assembled from existing regional geological maps; it has been widely used for constructing datasets (e.g. SoilGrids250m (Hengl, Mendes de Jesus et al. 2017)). However, the data quality of GLiM can vary in different spatial locations depending on the quality of the original regional geological maps. GLiM consists of three levels, the first level contains 16 lithological classes, and the additional two levels describe more specific lithological characteristics. For contiguous China, the compiled regional data sources (China 1991, Xinjiang 1992, Survey 2001) have slightly lower resolutions than the GLiM target resolution (1:1 000 000). However, for a basin-scale study with a mean basin area of over 2000 km^2, the classification accuracy should satisfy most applications.

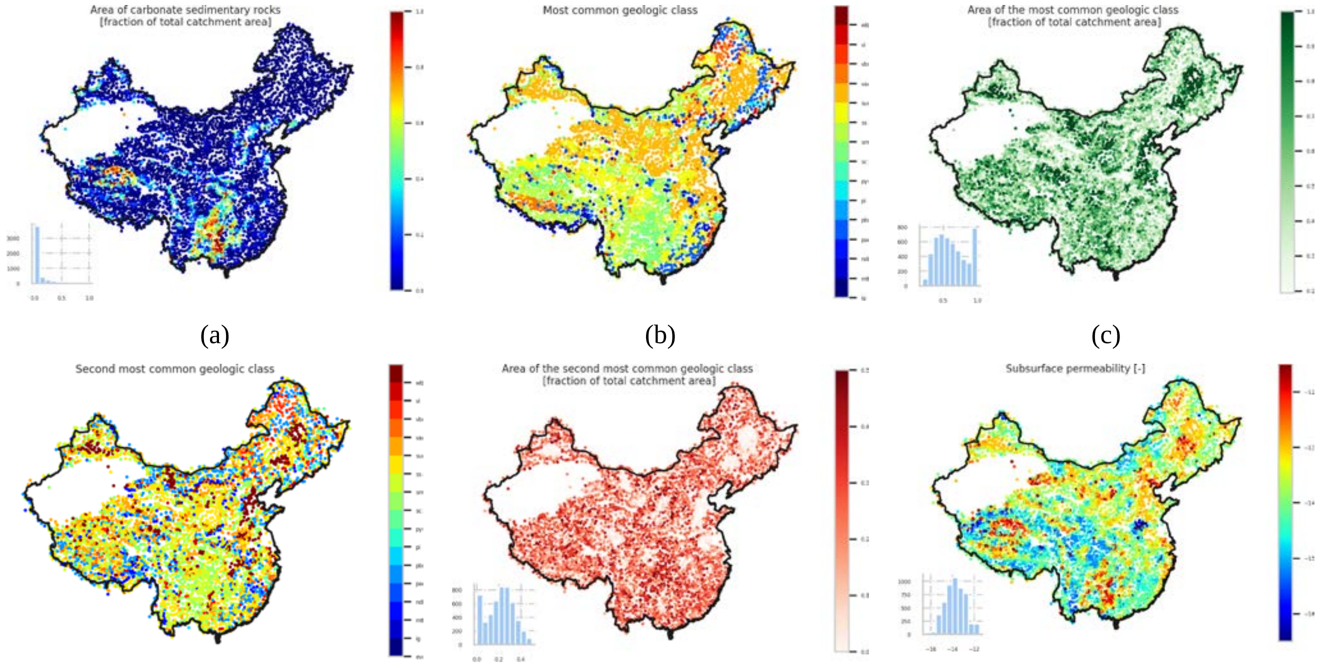
Area of carbonate sedimentary rocks
[fraction of total catchment area]
Most common geologic class
Area of the most common geologic class
[fraction of total catchment area]
Second most common geologic class
Area of the second most common geologic class
[fraction of total catchment area]
Subsurface permeability [-]

(a) (b) (c)

(a) (b) (c)

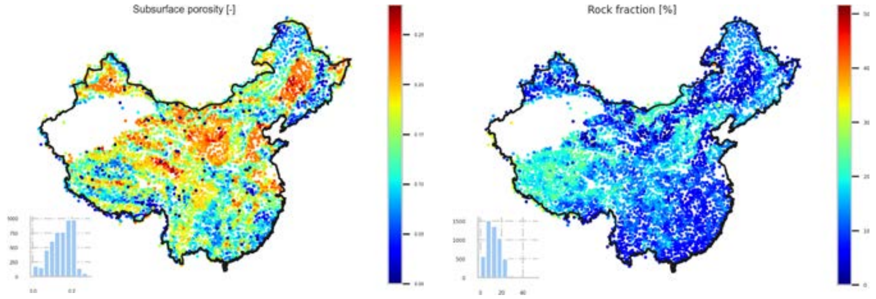

(a) (b)

Figure 4. Maps of geological characteristics over contiguous China. The histograms indicate the number of catchments (out of 4875) in each bin.

Compared to CAMELS and CAMELS-CL, one design consideration of the proposed dataset is that it should be more prepared for the data-driven research, such that we aim to generate as many types of catchment-scale data as possible since advanced data-driven methods can learn the representation of inputs automatically. To this end, we determined and recorded each lithological class's contribution to the catchment instead of recoding just the first and second most frequent classes. The GLiM is represented by 1,235,400 polygons; the polygons are converted to raster format for the basin-scale lithological type statistics.

GLobal HYdrogeology MaPS (GLHYMPS) provides a global estimation of subsurface permeability and porosity, two critical characteristics for the soils' hydrological classification. Porosity and permeability influence an area's infiltration capacity. Soil with high porosity is likely to contain s amounts of water, and high permeable soil transmits water relatively quickly. Based on the high-resolution map of GLiM, which can differentiate fine and coarse-grained sediments and sedimentary rocks, GLHYMPS determined subsurface permeability depending on the different permeabilities of rock types. For the proposed dataset, we calculated the catchment arithmetic mean for porosity. Followed (Gleeson, Smith et al. 2011), the logarithmic scale geometric mean is used for representing subsurface permeability. The summary of geological characteristics is present in Table 3.

Porosity and permeability have similar distributions as geological classes. These two characteristics are highly dependent on rock properties, unconsolidated sediments, mixed sedimentary rocks, siliciclastic sedimentary rocks, carbonate sedimentary rocks, and acid plutonic rocks are the five most common geological classes in contiguous China. Unconsolidated sediment is the most common rock type in contiguous China, dominating 31.9% of catchments; it extends from Xinjiang to the inland of the northeast and the coastal area surrounding the Bohai Sea, due to the high proportion of unconsolidated sediments present in the rock, these areas typically have high permeability and medium porosity. Mixed sedimentary rocks are the second most common rock type in contiguous China, accounting for 20.3% of catchments, it dominated the southern Qinghai-Tibet Plateau, western Yunnan-Guizhou Plateau, and northern Inner Mongolia. These areas typically have high porosity and low permeability. Siliciclastic sedimentary rocks dominate 17.7% of basins, mainly distributed in the northern part of the Qinghai-Tibet Plateau and the junction of the Qinghai-Tibet Plateau and the Yunnan-Guizhou Plateau; there are also some distributions in the eastern inland. These areas have low subsurface permeability and high subsurface porosity. Amongst all catchments, 9.8% of catchments are dominated by carbonate sedimentary rocks. Carbonate sedimentary rocks are mainly located in eastern Yunnan and northern Qinghai-Tibet Plateau. Acid plutonic rocks are typically distributed in the mountains surrounding the inland northeast, namely the Daxinganling Mountain and the hills in southern Guangdong and southwestern Guangxi. They are also distributed along the Brahmiputra river in the south part of the Qinghai-Tibet Plateau. The distribution of Acid plutonic rocks is relatively scattered; there are many isolated Acid plutonic rocks distributions in different locations of contiguous China, accompanied by medium permeability and high porosity.

In summary, the types of rocks in contiguous China are dominated by unconsolidated sediments and mixed sedimentary rocks. In 33.86% of the catchments, the dominant rock types occupy less than 50% of the catchment areas, and only 16.8% basins are having a dominant rock type with an area fraction greater than 90%. Amongst 4875 basins, 9.4% of basins have prevalent rock types wholly occupying the area.

5 Landcover

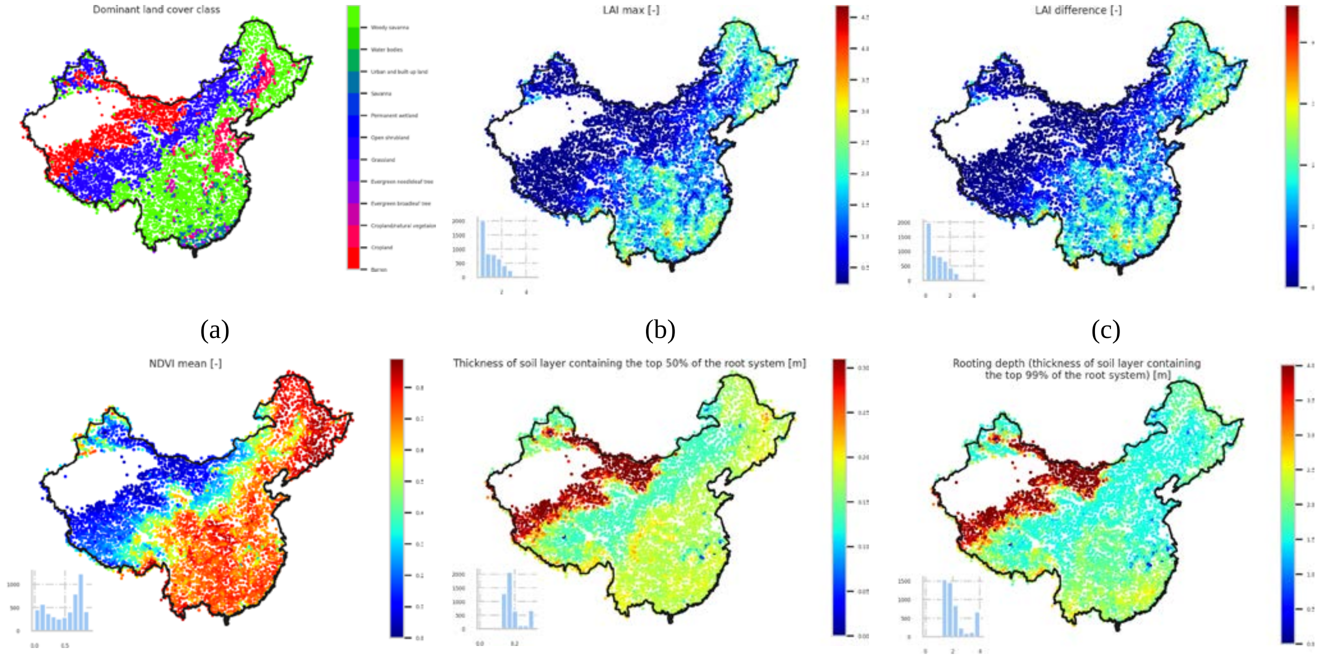
Dominant land cover class
Woody savanna
Water bodies
Urban and built-up land
Savanna
Permanent wetland
Open shrubland
Grassland
Evergreen needleleaf tree
Evergreen broadleaf tree
Cropland/natural vegetation
Cropland
Barren
LAI max [-]
LAI difference [-]
NDVI mean [-]
Thickness of soil layer containing the top 50% of the root system [m]
Rooting depth (thickness of soil layer containing the top 99% of the root system) [m]

(a) (b) (c)

(d) (e) (f)

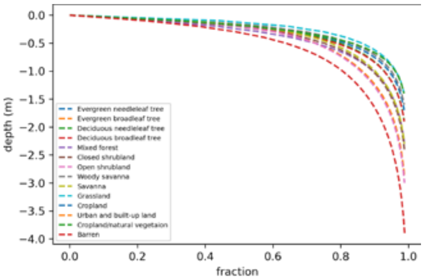

(g)

Figure 5. Maps of land cover characteristics over contiguous China. The histograms indicate the number of catchments (out of 4875) in each bin.

We selected two indicators to characterize vegetation density and growth on the surface: Normalized difference vegetation index (NDVI) and Leaf area index (LAI). NDVI is an indicator with a valid range of -0.2 to 1, assessing whether the area being observed contains live green vegetation or the plants' health. However, NDVI is just a qualitative measurement of the vegetation density; it cannot provide a quantitative estimate of the vegetation density in the area. Moreover, NDVI often provides inaccurate vegetation density measurements, and only long-term measurement and comparison can ensure its accuracy. NDVI alone is not enough to estimate the state of plants in an area. Therefore, we have selected another indicator, LAI, to supplement the deficiencies of NDVI.

LAI is defined as the total needle surface area per unit ground area and half of the entire needle surface area per unit ground surface area. It is a quantifiable value. It is functionally related to many hydrological processes like water interception (van Wijk and Williams 2005). (Buermann, Dong et al. 2001) verifies the validity of LAI used to characterize vegetation growth. The data sources used are The Terra Moderate Resolution Imaging Spectroradiometer (MODIS) Vegetation Indices (Didan 2015) for NDVI and Moderate Resolution Imaging Spectroradiometer (MODIS) (Myneni, Knyazikhin et al. 2015) for LAI. Followed (Addor, Newman et al. 2017), we determined maximum monthly LAI as an indicator characterising vegetation interception capacity and the maximum evaporative capacity and the difference between the maximum and minimum monthly LAI representing LAI's temporal variations.

Land cover classification refers to segmenting the ground into different categories based on remote sensing images. The Terra and Aqua combined Moderate Resolution Imaging Spectroradiometer (MODIS) Land Cover Type provides different results depending on the classification system used. Annual International Geosphere-Biosphere Programme (IGBP) classification is used for building the dataset, which is derived by the c4.5 decision tree algorithm. The IGBP classification system was formulated by the IGBP Land Cover Working Group in 1995, resulting in 17 categories of land cover types (Belward, Estes et al. 1999). (Friedl, Sulla-Menashe et al. 2010) compared the IGBP data of MODIS with other reference dataset and concluded that the MODIS classification of IGBP has an accuracy of 75%. We determined the fraction of each land cover class for each basin based on the Terra and Aqua combined Moderate Resolution Imaging Spectroradiometer (MODIS) Land Cover Type

(Sulla-Menashe and Friedl 2018), which differentiates our dataset from CAMELS and CAMELS-CL (only calculated the proportion of the dominant types).

Followed (Addor, Newman et al. 2017), we also computed the average rooting depth (50% and 90%) for each catchment based on the IGBP classification using a two-parameter method (Zeng 2001). The root depth distribution of vegetation affects the ground’s water holding capacity and the topsoil layer’s annual evapotranspiration (Desborough 1997). Many models use root depth as an essential parameter to characterize soil moisture absorption capacity. (Zeng 2001) developed a two-parameter asymptotic equation for estimating root depth distribution; the root depth distribution is global, derived based on the IGBP classification avoiding the problem of significantly different root distributions in various research. Figure 5(g) shows root depth distributions of different vegetation types, based on (Zeng 2001)‘s method. The 90% root depth is usually considered to be “rooting depth”, among the 17 categories of IGBP, cropland has the smallest rooting depth, and open shrubland has the largest. The 90% root depth of all vegetation is less than 2 meters. The national distribution of catchments soil characteristics is shown in Fig. 5.

6 Location and topography

The catchments’ boundary files are obtained from the global drainage basin dataset (Masutomi, Inui et al. 2009). The PDBD dataset was derived from digital elevation models (DEMs) with a high-resolution (100m-1km), and the errors were corrected by either automatic methods or manually. Additionally, PDBD also provides population and population density estimates for catchments, and these two indicators are also included in our dataset as a measure of human intervention. Global Runoff Data Centre (Center 2005) discharge gauging stations were used for referencing the derived basins. In contiguous China, PDBD has a high average match area rate (AMAR) and good geographic agreement with existing global drainage basin data. Based on the high-quality dataset, precise geographic and topographic information can be derived. See Fig. 6 for a summary.

The topography attributes of each catchment are determined based on the ASTGTM product retrieved from https://lpdaac.usgs.gov, maintained by the NASA EOSDIS Land Processes Distributed Active Archive Center (LP DAAC) at the USGS Earth Resources Observation and Science (EROS) Center.

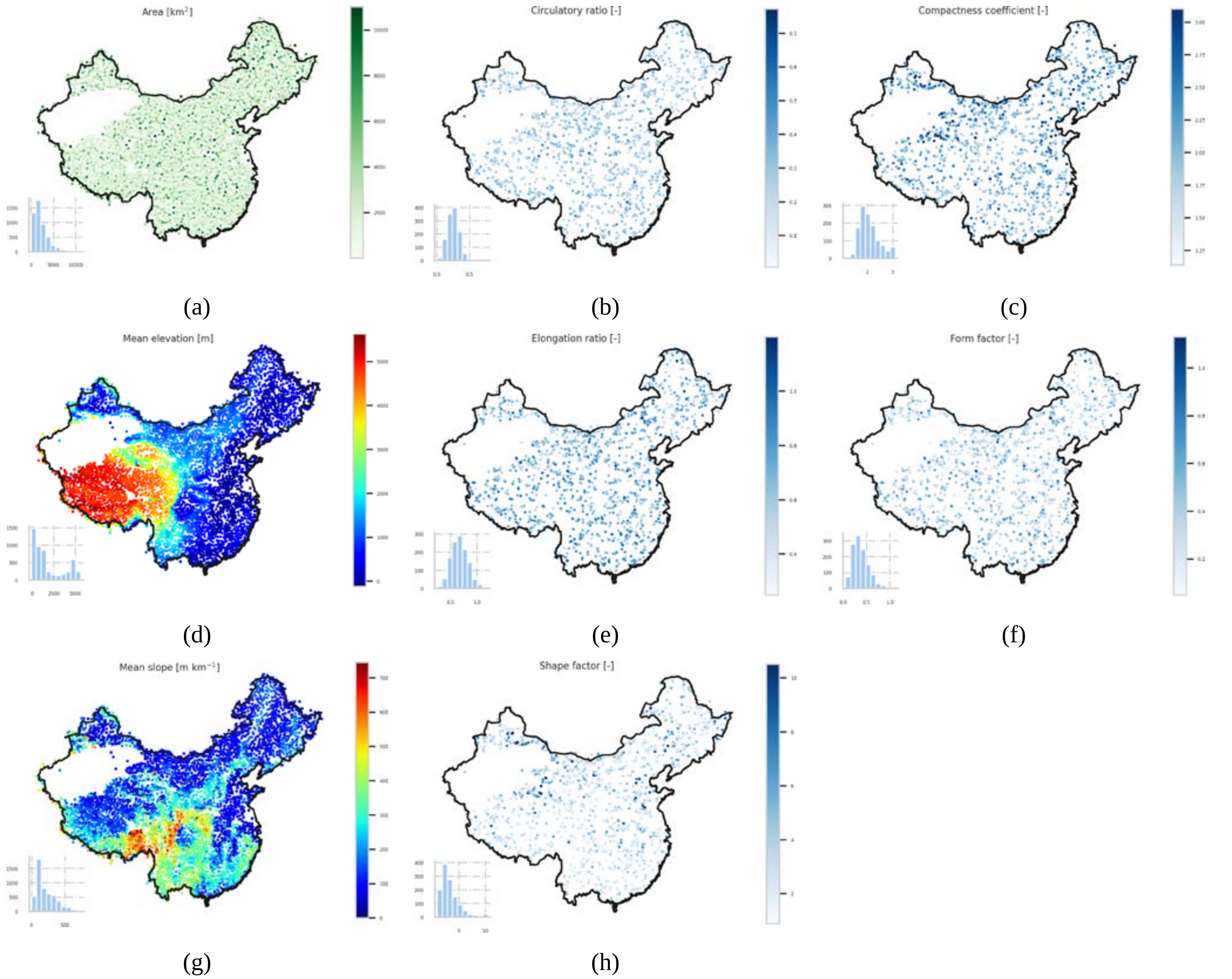

(a) (b) (c)

(d) (e) (f)

(g) (h)

Figure 6. Maps of topographic characteristics over contiguous China. The histograms indicate the number of catchments (out of 4875) in each bin.

The CAMELS dataset just provides two parameters (two area estimates) for describing the catchment shape; however, the physical characteristics of a catchment can affect the runoff volume and the runoff hydrograph of the catchment under a storm. To provide a complete description of the catchment shape, we computed several geometrical parameters of the catchment related to the runoff process, including catchment form factor, shape factor, compactness coefficient, circulatory ratio and the elongation ratio (Subramanya 2013). A summary of the location and topography attributes can be found in Table 3.

7 Soil

The proposed dataset has a total of 54 soil attributes (Table 3) derived from (Hengl, Mendes de Jesus et al. 2017), (Dai, Xin et al. 2019) and (Shangguan, Dai et al. 2013). The summary result is shown in Fig. 7. Five categories of soil characteristics (pH in H2O, organic carbon content, depth to bedrock, cation-exchange capacity, and bulk density) are determined from SoilGrids. SoilGrids (Hengl, Mendes de Jesus et al. 2017) provides global predictions for soil properties including organic carbon, bulk density, cation exchange capacity (CEC), pH, soil texture fractions and coarse fragments by fusing multiple data sources including MODIS land products, SRTM DEM, climatic images and global landform and lithology maps at the 250m resolution. SoilGrids made predictions based on machine learning algorithms and many covariates layers primarily derived from remote sensing data. SoilGrids has soil characteristics for several soil depths.

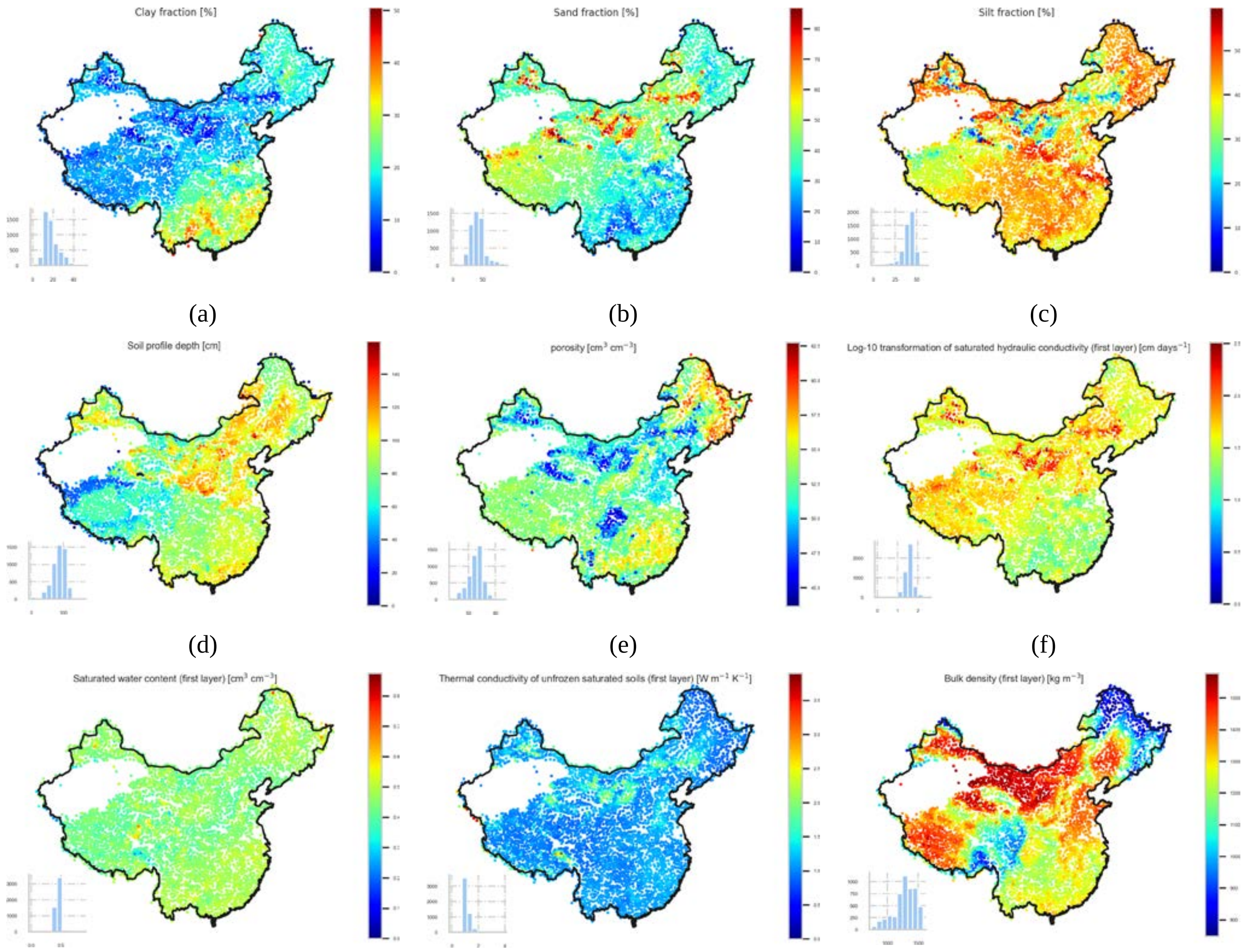
Clay fraction [%]
Sand fraction [%]
Silt fraction [%]
Soil profile depth [cm]
porosity [cm³ cm⁻³]
Log-10 transformation of saturated hydraulic conductivity (first layer) [cm days⁻¹]
Saturated water content (first layer) [cm³ cm⁻³]
Thermal conductivity of unfrozen saturated soils (first layer) [W m⁻¹ K⁻¹]
Bulk density (first layer) [kg m⁻³]

(a) (b) (c)

(d) (e) (f)

(g) (h) (i)

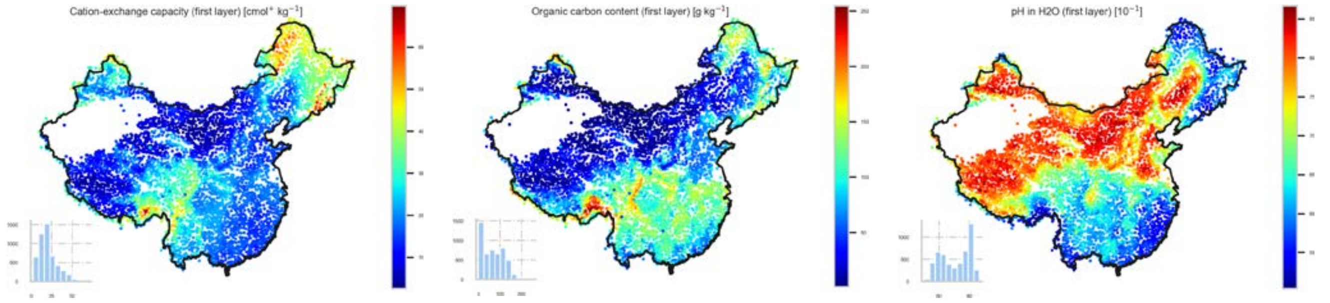
Cation-exchange capacity (first layer) [cmol+ kg−1]
Organic carbon content (first layer) [g kg−1]
pH in H2O (first layer) [10−1]

(j) (k) (l)

Figure 7. Maps of soil characteristics over contiguous China. The histograms indicate the number of catchments (out of 4875) in each bin.

Unlike CAMELS, whose reported results are obtained by a linear weighted combination of the different soil layers, and CAMELS-BR, whose products are soil characteristics at a depth of 30cm. We computed soil characteristics at all soil layers provided by SoilGrids such that advanced models can learn directly from the raw inputs.

To be consistent with CAMELS, we also determined saturated water content and saturated hydraulic conductivity (Dai, Xin et al. 2019). We also introduced thermal conductivity of unfrozen saturated soils (Dai, Xin et al. 2019). (Dai, Xin et al. 2019) provides a global estimation of soil hydraulic and thermal parameters using multiple Pedotransfer Functions (PTFs) based on SoilGrids. Based on the SoilGrids and GSDE (Shangguan, Dai et al. 2014) datasets, (Dai, Xin et al. 2019) produced six soil layers with a spatial resolution 30×30 arc-second. The vertical resolution of (Dai, Xin et al. 2019) is the same as the SoilGrids, with six intervals of 0–0.05 m, 0.05–0.15 m, 0.15–0.30 m, 0.30–0.60 m, 0.60–1.00 m, and 1.00–2.00 m. Same as the methods applied to SoilGrids, we determined and records catchment soil characteristics for all these layers.

To provide even more complete description of the soil, we determined seven more soil characteristics (Shangguan, Dai et al. 2013) including soil profile depth, porosity, clay/silt/sand content, rock fragment, and soil organic carbon content. (Shangguan, Dai et al. 2013) provides physical and chemical attributes of soils derived from 8979 soil profiles at 30×30 arc-second resolution, the polygon linkage method was used to derive the spatial distribution of soil properties. The profile attribute database and soil map are linked under a framework avoiding uncertainty in taxon referencing.

Depth to bedrock controls many physical and chemical processes in soil. The distribution of depth to bedrock in contiguous China is characterised by (i) low in the mountainous areas, such as Yunnan province and Chongqing City; (ii) high in barren areas, e.g. North and Northwest China. The introduced soil pH value is crucial since it influences many other physical and chemical soil characteristics. The spatial variability of soil pH in contiguous China is characterised by (i) soils in southern contiguous China are acid to strongly acid; (ii) soils in northern China are natural or alkaline; (iii) soils in north-eastern forested areas are also acid (pH < 7.2). Cation exchange capacity can be seen as a measure of soil fertility since it measures how much nutrient the soil can store such that it influences the growth of the vegetations. Cation exchange capacity is positively correlated with soil organic matter content and clay content, which Cation exchange capacity is generally low in sandy and silty soils. The spatial variability of Cation exchange capacity in contiguous China is characterised by (i) high in peat and forested areas in Qinghai-Tibet Plateau, central and northeast China (ii) The Cation exchange capacity in the desert area such as the northwest is extremely low. Soil hydraulic and thermal properties are greatly affected by soil organic matter (SOM). Soil organic matter has a similar distribution to the cation exchange capacity: high in the peat and forested areas such as northeast China and low in the north and northwest.

8 Meteorological time series

Table 4 Summary table of catchment meteorological time series available in the proposed dataset

Variable	Description	Unit
prs	catchment daily averaged ground pressure	hPa
tem	catchment daily averaged temperature at 2 m above ground	°C
rhu	catchment daily averaged relative humidity	-
pre	catchment daily averaged precipitation	mm d^{-1}
evp	catchment daily averaged evaporation measured by ground instruments	mm d^{-1}
win	catchment daily averaged wind speed at 2 m above ground	m s^{-1}
ssd	catchment daily averaged sunshine duration	h d^{-1}
gst	catchment daily averaged ground surface temperature	°C
pet	catchment daily averaged potential evapotranspiration determined by Penman's equation (see Appendix A)	mm d^{-1}

There have been many studies based on SURF_CLI_CHN_MUL_DAY in China (Liu, Xu et al. 2004, Xu, Gao et al. 2009, Huang, Han et al. 2016, Liu, Zheng et al. 2017), such as trend analysis of the pan evaporation (Liu, Yang et al. 2010). Still, there has not yet been a large-scale basin-oriented meteorological time series dataset in contiguous China. Researchers still need to do repeated works to extract historical meteorological data from the SURF_CLI_CHN_MUL_DAY dataset for the research. For the first time, we release a catchment-scale meteorological time series dataset. We will also open-source the code for researchers to generate any catchment's meteorological time series within contiguous China. The basin-oriented dataset provides meteorological time series for 4875 basins from 1990 to 2018 based on the China Meteorological Data Network. Meteorological time series includes pressure, temperature, relative humidity, precipitation, evaporation, wind speed, sunshine duration, ground surface temperature and potential evapotranspiration (see Table 4 for a summary).

The meteorological time series data from 1951 to 2010 is derived based on the "1951-2010 China National Ground Station Data Corrected Monthly Data File Basic Data Collection" data construction project. Other data include monthly reported data to the National Meteorological Information Centre by the provinces, and hourly and daily data uploaded by automatic ground stations in real-time. The SURF_CLI_CHN_MUL_DAY dataset is quality controlled, the quality and completeness of each variable are significantly improved compared to the previous similar products. M the development of the dataset, missing data were filled by interpolating its nearest stations.

Figure 2 presents the variation of the distribution of the observation sites. The start date of the recording is 1951, but because the early site distribution is sparse, we only used records from 1990 to 2018 to construct the dataset to ensure the data quality. The interpolation method used is the Inverse distance weighting since it shows better performance than other comparators. Catchment-scale raster is extracted from the interpolated national raster using the open-source rasterio[5] package. For all variables, we take the arithmetic mean on the extracted catchment raster as the catchment mean. Potential evapotranspiration (PET) is estimated based on Penman's Equation and other catchment meteorological variables.

9 Normal Camels YR – Normalized Catchment attributes and meteorology for Yellow River basin

Apart from the dataset providing the catchment attributes and meteorological forcing for contiguous China, we also offer a self-contained dataset covering the Yellow River basin with normalized streamflow measurements. The streamflow data are normalized to have zero mean and a standard deviation of 1 for each basin. The Normal-Camels-YR dataset is designed to support machine learning and deep learning research related to hydrology. In particular, fifty-four watersheds are less affected by human activities (selection is based on the Global Reservoirs and Dam databases (GRanD) (Lehner, Liermann et al. 2011) which provides the locations of reservoirs and dams globally), which makes them suitable for rainfall-runoff modelling research. For most machine learning and deep learning algorithms, data normalization will not affect model performance (e.g., neural network-based and tree-based algorithms). Besides, other research, such as trend analysis, can also be carried out. The Normal-Camels-YR dataset is self-contained to fully describe the Yellow River basin and is particularly helpful for the hydrology research of the Yellow River.

During the dataset development, basins with too few observations are removed, resulting in discontinuous basin identifiers. Normal-Camels-YR covers 102 gauges in the Yellow River basin, providing basin boundary shapefiles, static attributes and normalized streamflow measurements for each basin. The covered basins have areas ranging from 134 to 804,421 square kilometres. The time resolution of streamflow measurements is seven days, and the mean length of records of the streamflow measurements is 684, which means the mean period of the streamflow measurements for each basin is over 13 years.

[5] https://github.com/mapbox/rasterio

Meteorological variables included in Normal-Camels-YR is slightly different; it introduced daily maximum and minimum for some variables (Table 5).

Table 5 Meteorological variables provided in Normal-Camels-YR, the time series length is 22 years (1999-2020)

Attribute name	Description	Unit
evp	catchment daily averaged evaporation (observations)	0.1 mm d^{-1}
gst_mean	catchment daily averaged ground surface temperature	0.1 °C
gst_min	catchment daily minimum ground surface temperature	0.1 °C
gst_max	catchment daily maximum ground surface temperature	0.1 °C
pre	catchment daily averaged precipitation	0.1 mm d^{-1}
prs_mean	catchment daily averaged ground surface pressure	0.1 hPa
prs_max	catchment daily maximum ground surface pressure	0.1 hPa
prs_min	catchment daily minimum ground surface pressure	0.1 hPa
rhu	catchment daily averaged relative humidity	-
ssd	catchment daily averaged sunshine duration	0.1 h
tem_mean	catchment daily averaged temperature	0.1 °C
tem_min	catchment daily minimum temperature	0.1 °C
tem_max	catchment daily maximum temperature	0.1 °C
win_max	catchment daily maximum wind speed	0.1 m s^{-1}
win_mean	catchment daily averaged wind speed	0.1 m s^{-1}

10 Data availability and software packages used.

The proposed dataset is freely available at http://doi.org/10.5281/zenodo.4704017. The files provided are (i) several separate files containing 120+ catchments attributes, (ii) the daily meteorological time series in a zip file, (iii) the catchment boundaries used to compute the attributes and extract the time series, (iv) the Normal-Camels-YR dataset, (v) an attribute description file and (v) a readme file. The code used to generate the dataset is mainly based on several publicly available packages: rasterio, gdal[6], pyshp[7], geopandas[8], fiona[9], and xarray[10]. Complement code for generating any watershed's dataset will be released soon.

11 Conclusion

The dataset proposed in this paper provides a novel dataset for hydrological research in contiguous China. In the study area, there is no catchment attributes dataset has been proposed before, either a catchment-scale time series meteorological dataset. All catchments delaminated from the DEM are studied, covering contiguous China. The dataset includes daily meteorological forcing time-series data including precipitation, temperature, potential evapotranspiration, wind, ground surface temperature, pressure, humidity, sunshine duration and derived potential evapotranspiration of 4875 catchments. The proposed time series dataset is derived based on the quality-controlled site observation dataset, SURF_CLI_CHN_MUL_DAY. We will also release the complement code for generating any shapefile's meteorological time series within contiguous China based on the SURF_CLI_CHN_MUL_DAY dataset (freely available for Chinese researchers). The dataset has longer time series (from 1990 to 2018) and more meteorological variables than the previously proposed datasets. The dataset also includes 120+ catchment attributes, including soil, land cover, geology, climate indices and topography for each catchment. We produced a series of maps depicting the catchment attributes distributions in contiguous China. These maps present regional changes of various features; we also describe the relationships between them. The integration of multiple data sources into one dataset at a catchment-scale dramatically simplifies the data compilation process in research. Based on the dataset, we can test hypotheses and formulate valid conclusions under various conditions, not just limited to a few specific locations. Together with the Normal-Camels-YR dataset, the proposed dataset can help explore how different basin characteristics influence hydrological behaviours, learn the migration of hydrological behaviours between different basins, and to develop general frameworks for large-scale model evaluation and benchmarking in China.

Appendix A: Modified Penman's equation

Penman's equation (Subramanya 2013), incorporating some modifications to the original formula, is:

$$PET = \frac{AH_n + E_a\gamma}{A + \gamma}$$

[6] https://github.com/OSGeo/gdal

[7] https://github.com/GeospatialPython/pyshp

[8] https://github.com/geopandas/geopandas

[9] https://github.com/Toblerity/Fiona

[10] https://github.com/pydata/xarray

where PET is the daily potential evapotranspiration in mm per day; A is the slope of the saturation vapour pressure (ew) vs temperature (t) curve at the mean air temperature, in mm of mercury per Celsius; Hn is the net radiation in mm of evaporable water per day; Ea is a parameter including wind speed and saturation deficit; γ is the psychrometric constant = 0.49 mm of mercury per Celsius.

460

The relationship between ew and t is defined as:

$$e_w = 4.584 \exp\left(\frac{17.27t}{237.3 + t}\right)$$

The following equation estimates the net radiation:

$$H_n = H_a(1 - r)\left(a + b\frac{n}{N}\right) - \sigma T_a^4 \left(0.56 - 0.092\sqrt{e_a}\right)\left(0.10 + 0.90\frac{n}{N}\right)$$

465 where Ha is the incident solar radiation outside the atmosphere on a horizontal surface, expressed in mm of evaporable water per day (a function of the latitude and period of the year as indicated in Table A1); a is a constant depending upon the latitude ϕ and is given by $a = 0.29 \cos \phi$; b is a constant = 0.52; n is the sunshine duration in hours; N is the maximum possible hours of bright sunshine (a function of latitude, see Table A2); r is the reflection coefficient; σ is the Stefan-Boltzman constant = 2.01×10^{-9} mm/day; Ta is the mean air temperature in degrees kelvin; ea is the actual mean vapour pressure in the air in 470 mm of mercury.

Table A1. Mean Monthly Solar Radiation, *Ha* in mm of Evaporable Water/Day

North latitude	Jan	Feb	Mar	Apr	May	Jun	Jul	Aug	Sep	Oct	Nov	Dec
0°	14.5	15.0	15.2	14.7	13.9	13.4	13.5	14.2	14.9	15.0	14.6	14.3
10°	12.8	13.9	14.8	15.2	15.0	14.8	14.8	15.0	14.9	14.1	13.1	12.4
20°	10.8	12.3	13.9	15.2	15.7	15.8	15.7	15.3	14.4	12.9	11.2	10.3
30°	8.5	10.5	12.7	14.8	16.0	16.5	16.2	15.3	13.5	11.3	9.1	7.9
40°	6.0	8.3	11.0	13.9	15.9	16.7	16.3	14.8	12.2	9.3	6.7	5.4
50°	3.6	5.9	9.1	12.7	15.4	16.7	16.1	13.9	10.5	7.1	4.3	3.0

The parameter Ea is estimated as:

$$E_a = 0.35\left(1 + \frac{u_2}{160}\right)(e_w - e_a)$$

475 where $u2$ is the wind speed at $2m$ above ground in km/day; ew is the saturation vapour pressure at mean air temperature in mm of mercury; ea is the actual vapour pressure.

Table A2. Mean Monthly Values of Possible Sunshine Hours, *N*

North latitude	Jan	Feb	Mar	Apr	May	Jun	Jul	Aug	Sep	Oct	Nov	Dec
0°	12.1	12.1	12.1	12.1	12.1	12.1	12.1	12.1	12.1	12.1	12.1	12.1

10°	11.6	11.8	12.1	12.4	12.6	12.7	12.6	12.4	12.9	11.9	11.7	11.5
20°	11.1	11.5	12.0	12.6	13.1	13.3	13.2	12.8	12.3	11.7	11.2	10.9
30°	10.4	11.1	12.0	12.9	13.7	14.1	13.9	13.2	12.4	11.5	10.6	10.2
40°	9.6	10.7	11.9	13.2	14.4	15.0	14.7	13.8	12.5	11.2	10.0	9.4
50°	8.6	10.1	11.8	13.8	15.4	16.4	16.0	14.5	12.7	10.8	9.1	8.1

Appendix B: Correlation analysis of catchment attributes

To explore the potential connections between various types of watershed attributes, we did correlation analysis using the Pearson correlation coefficient; the results can be found in Table B1, which shows the top five most relevant attributes for each attribute, and the Fig. S1, the correlation matrix. The analysis result shows that the correlations between variables are consistent with general understanding, justifying the rationality of the dataset:

(1) Subsurface permeability and porosity are highly correlated with geological attributes.

(2) LAI and NDVI have a high positive correlation (0.866).

(3) Root depth is most correlated with land cover types.

(4) In China, the savanna is mainly distributed in the southern coastal areas, resulting in that it is positively correlated with average rainfall (0.604).

(5) Sand is positively correlated with saturated hydraulic conductivity (0.86) while the clay is negatively correlated (-0.763), and catchments with a lot of rainfall are less likely to have soil with high hydraulic conductivity (-0.647).

(6) High altitude catchments tend to have lower saturated water content (-0.705).

Table B1. The top five most relevant characteristics for each attribute (different soil layers for the same attribute are excluded, e.g. phihox_sl2 is not included in the top five most relevant attributes of phihox_sl1 though they are highly correlated)

Attribute	1st	2nd	3rd	4th	5th
high_prec_freq	low_prec_dur(-0.58)	root_depth_50(-0.438)	root_depth_99(-0.436)	barren(-0.39)	pet_mean(-0.261)
high_prec_dur	elev(0.544)	theta_s_l6(-0.503)	prs_mean (-0.49)	theta_s_l5(-0.458)	rhu_mean(-0.431)
low_prec_freq	pre_mean(-0.881)	ssd_mean(0.841)	phihox_sl7(0.825)	phihox_sl6(0.818)	phihox_sl5(0.814)
low_prec_dur	barren(0.728)	rhu_mean(-0.723)	evp_mean(0.721)	ndvi_mean(-0.684)	root_depth_99(0.66)
frac_snow_daily	tem_mean(-0.951)	gst_mean(-0.949)	ssd_mean(0.777)	pre_mean(-0.762)	n_min(0.703)
p_seasonality	pre_mean(0.901)	rhu_mean(0.765)	ssd_mean(-0.764)	low_prec_freq(-0.712)	frac_snow_daily(-0.683)
pet_mean	cecsol_sl2(-0.66)	cecsol_sl1(-0.634)	cecsol_sl3(-0.628)	gst_mean(0.622)	bldfie_sl1(0.608)
pre_mean	p_seasonality(0.901)	low_prec_freq(-0.881)	ssd_mean(-0.858)	rhu_mean(0.832)	phihox_sl7(-0.819)
tem_mean	gst_mean(0.992)	frac_snow_daily(-0.951)	pre_mean(0.747)	ssd_mean(-0.709)	p_seasonality(0.681)
prs_mean	elev(-0.889)	e_max(0.707)	lon(0.707)	e_min(0.707)	rhu_mean(0.603)

rhu_mean	ssd_mean(-0.887)	pre_mean(0.832)	evp_mean(-0.823)	ndvi_mean(0.813)	low_prec_freq(-0.803)
evp_mean	ndvi_mean(-0.845)	rhu_mean(-0.823)	ssd_mean(0.756)	e_min(-0.731)	lon(-0.73)
win_mean	ssd_mean(0.581)	frac_snow_daily(0.571)	tem_mean(-0.52)	gst_mean(-0.507)	low_prec_freq(0.477)
ssd_mean	rhu_mean(-0.887)	pre_mean(-0.858)	low_prec_freq(0.841)	frac_snow_daily(0.777)	p_seasonality(-0.764)
gst_mean	tem_mean(0.992)	frac_snow_daily(-0.949)	pre_mean(0.743)	n_min(-0.693)	lat(-0.693)
geol_permeability	ss(-0.408)	sm(-0.403)	su(0.399)	sc(0.323)	bdticm(0.24)
geol_porosity	su(0.627)	pa(-0.575)	phihox_sl1(0.46)	phihox_sl3(0.454)	phihox_sl4(0.453)
ig	snow and ice(0.471)	tksatu_l5(0.324)	tksatu_l3(0.318)	tksatu_l4(0.306)	tksatu_l2(0.275)
pa	geol_porosity(-0.575)	phihox_sl1(-0.314)	phihox_sl3(-0.302)	phihox_sl2(-0.301)	phihox_sl4(-0.297)
sc	geol_porosity(-0.362)	geol_permeability(0.323)	n_max(-0.317)	lat(-0.317)	n_min(-0.316)
su	geol_porosity(0.627)	bdticm(0.599)	cropland(0.468)	phihox_sl1(0.44)	phihox_sl4(0.439)
sm	geol_permeability(-0.403)	su(-0.385)	cropland(-0.268)	bdticm(-0.233)	e_max(-0.228)
vi	deciduous broadleaf tree(0.214)	geol_porosity(-0.18)	lai_max(0.165)	lai_dif(0.159)	e_max(0.157)
mt	geol_porosity(-0.412)	evergreen needleleaf tree(0.327)	orcdrc_sl3(0.265)	orcdrc_sl4(0.258)	bldfie_sl5(-0.254)
ss	geol_permeability(-0.408)	su(-0.287)	sm(-0.206)	geol_porosity(0.2)	tksatu_l6(-0.156)
pi	deciduous broadleaf tree(0.299)	geol_porosity(-0.208)	e_max(0.161)	lon(0.161)	e_min(0.16)
va	geol_porosity(-0.218)	high_prec_dur(0.191)	tem_mean(-0.167)	gst_mean(-0.16)	su(-0.16)
wb	water bodies(0.674)	permanent wetland(0.379)	root_depth_50(-0.164)	theta_s_l3(0.148)	theta_s_l4(0.147)
pb	theta_s_l6(-0.137)	theta_s_l5(-0.133)	elev(m)(0.124)	theta_s_l4(-0.114)	prs_mean(-0.102)
vb	cecsol_sl2(0.222)	cecsol_sl3(0.213)	cecsol_sl1(0.212)	cecsol_sl4(0.211)	cecsol_sl5(0.208)
nd	snow and ice(0.206)	theta_s_l2(-0.154)	theta_s_l3(-0.151)	theta_s_l1(-0.144)	tksatu_l4(0.136)
py	phihox_sl1(-0.214)	phihox_sl2(-0.207)	phihox_sl3(-0.207)	phihox_sl4(-0.205)	phihox_sl5(-0.202)
ev	tksatu_l3(0.07)	tksatu_l4(0.066)	barren(0.064)	tksatu_l2(0.061)	tksatu_l1(0.061)
lai_dif	ndvi_mean(0.866)	phihox_sl4(-0.809)	phihox_sl2(-0.807)	phihox_sl5(-0.807)	phihox_sl6(-0.807)
lai_max	ndvi_mean(0.856)	phihox_sl4(-0.815)	phihox_sl5(-0.814)	phihox_sl6(-0.814)	phihox_sl2(-0.813)
ndvi_mean	lai_dif(0.866)	lai_max(0.856)	evp_mean(-0.845)	rhu_mean(0.813)	barren(-0.772)
root_depth_50	barren(0.856)	low_prec_dur(0.626)	grassland(-0.537)	ndvi_mean(-0.513)	evp_mean(0.497)

root_depth_99	barren(0.897)	low_prec_dur(0.66)	ndvi_mean(-0.628)	evp_mean(0.604)	rhu_mean(-0.486)
evergreen needleleaf tree	slope(0.398)	bldfie_sl4(-0.391)	bldfie_sl5(-0.384)	bldfie_sl3(-0.372)	bldfie_sl7(-0.366)
evergreen broadleaf tree	pre_mean(0.504)	lai_max(0.483)	phihox_sl7(-0.477)	lai_dif(0.471)	phihox_sl6(-0.47)
deciduous needleleaf tree	woody savanna(0.241)	cecsol_sl2(0.231)	orcdrc_sl2(0.226)	pet_mean(-0.215)	bldfie_sl1(-0.214)
deciduous broadleaf tree	lai_max(0.459)	lai_dif(0.452)	cecsol_sl1(0.433)	bldfie_sl1(-0.413)	e_max(0.361)
mixed forest	orcdrc_sl1(0.501)	lai_max(0.471)	lai_dif(0.466)	phihox_sl6(-0.462)	phihox_sl7(-0.461)
closed shrubland	theta_s_l1(-0.084)	grav(0.079)	sc(0.075)	theta_s_l2(-0.072)	urban and built-up land(0.064)
open shrubland	high_prec_dur(0.155)	theta_s_l6(-0.151)	rhu_mean(-0.149)	prs_mean(-0.147)	evp_mean(0.139)
woody savanna	lai_max(0.633)	lai_dif(0.631)	phihox_sl7(-0.592)	phihox_sl6(-0.59)	phihox_sl5(-0.585)
savanna	pre_mean(0.604)	phihox_sl7(-0.55)	clay(0.547)	phihox_sl6(-0.543)	phihox_sl5(-0.537)
grassland	root_depth_50(-0.537)	tem_mean(-0.496)	gst_mean(-0.491)	frac_snow_daily(0.469)	phihox_sl6(0.438)
permanent wetland	wb(0.379)	water bodies(0.349)	p_seasonality(0.3)	pre_mean(0.248)	pop_dnsty(0.23)
cropland	su(0.468)	lon(0.412)	e_min(0.412)	e_max(0.412)	elev(-0.388)
urban and built-up land	pop_dnsty(0.811)	pop(0.399)	p_seasonality(0.286)	tem_mean(0.261)	elev(-0.244)
cropland/natural vegetaion	ssd_mean(-0.458)	savanna(0.381)	rhu_mean(0.371)	frac_snow_daily(-0.367)	tem_mean(0.364)
snow and ice	tksatu_l5(0.568)	tksatu_l3(0.561)	tksatu_l4(0.533)	tksatu_l2(0.506)	tksatu_l1(0.503)
barren	root_depth_99(0.897)	root_depth_50(0.856)	ndvi_mean(-0.772)	low_prec_dur(0.728)	evp_mean(0.698)
water bodies	wb(0.674)	permanent wetland(0.349)	root_depth_50(-0.192)	root_depth_99(-0.154)	theta_s_l3(0.153)
length	area(0.849)	circulatory_ratio(-0.491)	elongation_ratio(-0.451)	form_factor(-0.436)	compactness_coefficient(0.292)
area	length(0.849)	pop(0.418)	circulatory_ratio(-0.255)	cecsol_sl1(0.142)	bldfie_sl2(-0.138)
form_factor	elongation_ratio(0.992)	circulatory_ratio(0.647)	shape_factor(-0.506)	length(-0.436)	compactness_coefficient(-0.383)
shape_factor	compactness_coefficient(0.786)	elongation_ratio(-0.566)	form_factor(-0.506)	circulatory_ratio(-0.372)	length(0.266)
compactness_coefficient	shape_factor(0.786)	circulatory_ratio(-0.594)	elongation_ratio(-0.421)	form_factor(-0.383)	length(0.292)

circulatory_ratio	elongation_ratio(0.651)	form_factor(0.647)	compactness_coefficient(-0.594)	length(-0.491)	shape_factor(-0.372)
elongation_ratio	form_factor(0.992)	circulatory_ratio(0.651)	shape_factor(-0.566)	length(-0.451)	compactness_coefficient(-0.421)
elev(m)	prs_mean(-0.889)	e_min(-0.753)	lon(-0.752)	e_max(-0.752)	theta_s_l4(-0.7)
slope(m/km)	n_min(-0.552)	lat(-0.551)	n_max(-0.55)	phihox_sl7(-0.491)	orcdrc_sl1(0.49)
n_min	lat(1.0)	frac_snow_daily(0.703)	gst_mean(-0.693)	pre_mean(-0.651)	tem_mean(-0.648)
n_max	lat(1.0)	frac_snow_daily(0.701)	gst_mean(-0.692)	pre_mean(-0.65)	tem_mean(-0.647)
e_min	lon(1.0)	elev(-0.753)	evp_mean(-0.731)	prs_mean(0.707)	ndvi_mean(0.691)
e_max	lon(1.0)	elev(-0.752)	evp_mean(-0.729)	prs_mean(0.707)	ndvi_mean(0.69)
pop(people)	area(0.418)	urban and built-up land(0.399)	tem_mean(0.318)	p_seasonality(0.317)	frac_snow_daily(-0.304)
pop_dnsty(people/km^2)	urban and built-up land(0.811)	p_seasonality(0.426)	tem_mean(0.412)	gst_mean(0.395)	frac_snow_daily(-0.39)
lon	e_max(1.0)	e_min(1.0)	elev(-0.752)	evp_mean(-0.73)	prs_mean(0.707)
lat	n_min(1.0)	n_max(1.0)	frac_snow_daily(0.702)	gst_mean(-0.693)	pre_mean(-0.651)
tksatu_l1	snow and ice(0.503)	silt(-0.465)	som(-0.366)	sand(0.362)	log_k_s_l5(0.327)
tksatu_l2	snow and ice(0.506)	silt(-0.49)	sand(0.406)	som(-0.365)	log_k_s_l5(0.364)
tksatu_l3	snow and ice(0.561)	silt(-0.489)	sand(0.409)	ndvi_mean(-0.368)	clay(-0.334)
tksatu_l4	snow and ice(0.533)	silt(-0.49)	sand(0.465)	ndvi_mean(-0.455)	log_k_s_l5(0.414)
tksatu_l5	snow and ice(0.568)	silt(-0.402)	ndvi_mean(-0.375)	sand(0.348)	lai_dif(-0.326)
tksatu_l6	snow and ice(0.449)	bdticm(0.403)	log_k_s_l6(0.384)	su(0.38)	low_prec_freq(0.36)
log_k_s_l1	sand(0.858)	clay(-0.733)	pre_mean(-0.553)	phihox_sl7(0.551)	phihox_sl6(0.546)
log_k_s_l2	sand(0.86)	clay(-0.729)	phihox_sl7(0.575)	phihox_sl6(0.569)	pre_mean(-0.568)
log_k_s_l3	sand(0.859)	clay(-0.728)	pre_mean(-0.571)	phihox_sl7(0.571)	phihox_sl6(0.565)
log_k_s_l4	sand(0.82)	clay(-0.752)	pre_mean(-0.647)	phihox_sl7(0.636)	phihox_sl6(0.63)
log_k_s_l5	sand(0.773)	clay(-0.714)	phihox_sl7(0.654)	phihox_sl6(0.649)	phihox_sl5(0.646)
log_k_s_l6	sand(0.688)	clay(-0.687)	phihox_sl7(0.665)	phihox_sl6(0.662)	pre_mean(-0.662)
theta_s_l1	grav(-0.705)	elev(-0.422)	rhu_mean(0.407)	clay(0.401)	pdep(0.4)
theta_s_l2	grav(-0.713)	elev(-0.505)	pdep(0.475)	e_min(0.442)	lon(0.441)
theta_s_l3	grav(-0.662)	elev(-0.638)	prs_mean(0.554)	pdep(0.52)	e_min(0.516)
theta_s_l4	elev(-0.7)	grav(-0.663)	prs_mean(0.594)	pdep(0.571)	e_min(0.51)
theta_s_l5	elev(-0.656)	grav(-0.584)	prs_mean(0.536)	pdep(0.501)	rhu_mean(0.467)
theta_s_l6	elev(-0.637)	prs_mean(0.525)	grav(-0.513)	high_prec_dur(-0.503)	rhu_mean(0.475)
orcdrc_sl7	cecsol_sl2(0.758)	bldfie_sl2(-0.745)	bldfie_sl4(-0.744)	bldfie_sl1(-0.737)	cecsol_sl3(0.735)
orcdrc_sl3	bldfie_sl2(-0.876)	bldfie_sl4(-0.875)	bldfie_sl3(-0.874)	bldfie_sl5(-0.849)	bldfie_sl1(-0.848)
orcdrc_sl4	bldfie_sl4(-0.823)	bldfie_sl2(-0.809)	bldfie_sl3(-0.803)	bldfie_sl5(-0.803)	bldfie_sl1(-0.787)

orcdrc_sl5	bldfie_sl4(-0.759)	bldfie_sl2(-0.754)	bldfie_sl5(-0.745)	bldfie_sl1(-0.745)	bldfie_sl3(-0.731)
orcdrc_sl6	cecsol_sl2(0.733)	bldfie_sl4(-0.733)	bldfie_sl2(-0.728)	bldfie_sl1(-0.725)	bldfie_sl5(-0.721)
orcdrc_sl2	bldfie_sl2(-0.917)	bldfie_sl1(-0.908)	bldfie_sl3(-0.861)	cecsol_sl1(0.854)	bldfie_sl4(-0.854)
orcdrc_sl1	phihox_sl2(-0.826)	phihox_sl1(-0.824)	phihox_sl3(-0.822)	phihox_sl4(-0.819)	phihox_sl5(-0.813)
phihox_sl7	low_prec_freq(0.825)	pre_mean(-0.819)	lai_max(-0.806)	orcdrc_sl1(-0.804)	lai_dif(-0.799)
phihox_sl6	low_prec_freq(0.818)	lai_max(-0.814)	pre_mean(-0.81)	orcdrc_sl1(-0.807)	lai_dif(-0.807)
phihox_sl5	lai_max(-0.814)	low_prec_freq(0.814)	orcdrc_sl1(-0.813)	lai_dif(-0.807)	pre_mean(-0.801)
phihox_sl4	orcdrc_sl1(-0.819)	lai_max(-0.815)	lai_dif(-0.809)	low_prec_freq(0.804)	pre_mean(-0.781)
phihox_sl3	orcdrc_sl1(-0.822)	lai_max(-0.813)	lai_dif(-0.806)	low_prec_freq(0.799)	pre_mean(-0.772)
phihox_sl2	orcdrc_sl1(-0.826)	lai_max(-0.813)	lai_dif(-0.807)	low_prec_freq(0.798)	pre_mean(-0.767)
phihox_sl1	orcdrc_sl1(-0.824)	lai_max(-0.804)	lai_dif(-0.798)	low_prec_freq(0.78)	pre_mean(-0.741)
bldfie_sl7	orcdrc_sl3(-0.775)	orcdrc_sl4(-0.747)	orcdrc_sl5(-0.698)	orcdrc_sl2(-0.698)	orcdrc_sl6(-0.671)
bldfie_sl6	orcdrc_sl3(-0.776)	orcdrc_sl4(-0.748)	orcdrc_sl5(-0.701)	orcdrc_sl2(-0.694)	orcdrc_sl6(-0.677)
bldfie_sl5	orcdrc_sl3(-0.849)	orcdrc_sl2(-0.81)	orcdrc_sl4(-0.803)	orcdrc_sl5(-0.745)	orcdrc_sl7(-0.728)
bldfie_sl4	orcdrc_sl3(-0.875)	orcdrc_sl2(-0.854)	orcdrc_sl4(-0.823)	cecsol_sl1(-0.763)	orcdrc_sl5(-0.759)
bldfie_sl1	orcdrc_sl2(-0.908)	cecsol_sl1(-0.891)	orcdrc_sl3(-0.848)	cecsol_sl2(-0.828)	orcdrc_sl4(-0.787)
bldfie_sl3	orcdrc_sl3(-0.874)	orcdrc_sl2(-0.861)	orcdrc_sl4(-0.803)	cecsol_sl1(-0.795)	som(-0.787)
bldfie_sl2	orcdrc_sl2(-0.917)	orcdrc_sl3(-0.876)	cecsol_sl1(-0.87)	orcdrc_sl4(-0.809)	som(-0.808)
cecsol_sl1	bldfie_sl1(-0.891)	bldfie_sl2(-0.87)	orcdrc_sl2(0.854)	bldfie_sl3(-0.795)	orcdrc_sl3(0.781)
cecsol_sl2	bldfie_sl1(-0.828)	orcdrc_sl2(0.822)	bldfie_sl2(-0.798)	orcdrc_sl7(0.758)	orcdrc_sl3(0.746)
cecsol_sl5	bldfie_sl1(-0.681)	orcdrc_sl2(0.664)	orcdrc_sl7(0.649)	bldfie_sl2(-0.645)	orcdrc_sl6(0.636)
cecsol_sl4	bldfie_sl1(-0.72)	orcdrc_sl2(0.717)	orcdrc_sl7(0.693)	bldfie_sl2(-0.692)	orcdrc_sl6(0.679)
cecsol_sl3	bldfie_sl1(-0.784)	orcdrc_sl2(0.776)	bldfie_sl2(-0.76)	orcdrc_sl7(0.735)	orcdrc_sl3(0.733)
cecsol_sl7	bldfie_sl1(-0.661)	orcdrc_sl7(0.654)	orcdrc_sl2(0.642)	orcdrc_sl6(0.64)	orcdrc_sl5(0.619)
cecsol_sl6	bldfie_sl1(-0.648)	orcdrc_sl2(0.637)	orcdrc_sl7(0.632)	orcdrc_sl6(0.62)	bldfie_sl2(-0.61)
bdticm	su(0.599)	low_prec_freq(0.463)	log_k_s_l6(0.439)	phihox_sl2(0.437)	phihox_sl7(0.436)
pdep	elev(-0.662)	theta_s_l4(0.571)	e_min(0.566)	lon(0.565)	e_max(0.564)
por	silt(0.573)	clay(0.366)	tksatu_l2(-0.317)	som(0.314)	tksatu_l1(-0.309)
clay	pre_mean(0.763)	log_k_s_l4(-0.752)	log_k_s_l1(-0.733)	log_k_s_l2(-0.729)	log_k_s_l3(-0.728)

sand	log_k_s_l2(0.86)	log_k_s_l3(0.859)	log_k_s_l1(0.858)	log_k_s_l4(0.82)	log_k_s_l5(0.773)
silt	por(0.573)	sand(-0.558)	log_k_s_l3(-0.557)	log_k_s_l2(-0.547)	log_k_s_l1(-0.545)
grav	theta_s_l2(-0.713)	theta_s_l1(-0.705)	theta_s_l4(-0.663)	theta_s_l3(-0.662)	theta_s_l5(-0.584)
som	bldfie_sl2(-0.808)	bldfie_sl3(-0.787)	bldfie_sl1(-0.759)	bldfie_sl4(-0.747)	orcdrc_sl2(0.74)

Financial support

This research has been supported by the National Key Research and Development Program (2018YFC0407901, 2018YFC0407905), the National Natural Science Fund of China (51779100), and the Central Public-interest Scientific Institution Basal Research Fund (HKY-JBYW-2020-21, HKY-JBYW-2020-07).

References

Abu-Mostafa, Y. S., M. Magdon-Ismail and H.-T. Lin (2012). Learning from data, AMLBook New York, NY, USA:.

Addor, N., H. X. Do, C. Alvarez-Garreton, G. Coxon, K. Fowler and P. A. J. H. S. J. Mendoza (2020). "Large-sample hydrology: recent progress, guidelines for new datasets and grand challenges." **65**(5): 712-725.

Addor, N., A. J. Newman, N. Mizukami and M. P. Clark (2017). "The CAMELS data set: catchment attributes and meteorology for large-sample studies." Hydrology and Earth System Sciences (HESS) **21**(10): 5293-5313.

Alvarez-Garreton, C., P. A. Mendoza, J. P. Boisier, N. Addor, M. Galleguillos, M. Zambrano-Bigiarini, A. Lara, G. Cortes, R. Garreaud and J. McPhee (2018). "The CAMELS-CL dataset: catchment attributes and meteorology for large sample studies-Chile dataset." Hydrology and Earth System Sciences **22**(11): 5817-5846.

Belward, A. S., J. E. Estes and K. D. Kline (1999). "The IGBP-DIS global 1-km land-cover data set DISCover: A project overview." Photogrammetric Engineering and Remote Sensing **65**(9): 1013-1020.

Berghuijs, W. R., E. E. Aalbers, J. R. Larsen, R. Trancoso and R. A. Woods (2017). "Recent changes in extreme floods across multiple continents." Environmental Research Letters **12**(11): 114035.

Blume, T., I. van Meerveld and M. Weiler (2018). "Incentives for field hydrology and data sharing: collaboration and compensation: reply to “A need for incentivizing field hydrology, especially in an era of open data”." Hydrological Sciences Journal **63**(8): 1266-1268.

Blumer, A., A. Ehrenfeucht, D. Haussler and M. K. Warmuth (1987). "Occam’s razor." Information processing letters **24**(6): 377-380.

Brodeur, Z. P., J. D. Herman and S. Steinschneider (2020). "Bootstrap Aggregation and Cross-Validation Methods to Reduce Overfitting in Reservoir Control Policy Search." Water Resources Research **56**(8): e2020WR027184.

Buermann, W., J. Dong, X. Zeng, R. B. Myneni and R. E. Dickinson (2001). "Evaluation of the utility of satellite-based vegetation leaf area index data for climate simulations." Journal of Climate **14**(17): 3536-3550.

Center, G. G. R. D. (2005). Global Runoff Database, Koblenz.

Ceola, S., B. Arheimer, E. Baratti, G. Blöschl, R. Capell, A. Castellarin, J. Freer, D. Han, M. Hrachowitz, Y. J. H. Hundecha and E. S. Sciences (2015). "Virtual laboratories: new opportunities for collaborative water science." **19**(4): 2101-2117.

Chagas, V. B., P. L. Chaffe, N. Addor, F. M. Fan, A. S. Fleischmann, R. C. Paiva and V. A. Siqueira (2020). "CAMELS-BR: hydrometeorological time series and landscape attributes for 897 catchments in Brazil." Earth System Science Data **12**(3): 2075-2096.

China, M. o. G. a. M. R. o. t. P. s. R. o. (1991). "Geological map of Nei Mongol Autonomous Region, People’s Republic of China, scale 1:1,500,000."

Coron, L., V. Andreassian, C. Perrin, J. Lerat, J. Vaze, M. Bourqui and F. Hendrickx (2012). "Crash testing hydrological models in contrasted climate conditions: An experiment on 216 Australian catchments." Water Resources Research **48**(5).

Coxon, G., N. Addor, J. P. Bloomfield, J. Freer, M. Fry, J. Hannaford, N. J. Howden, R. Lane, M. Lewis and E. L. Robinson (2020). "CAMELS-GB: hydrometeorological time series and landscape attributes for 671 catchments in Great Britain." Earth System Science Data **12**(4): 2459-2483.

Dai, Y., Q. Xin, N. Wei, Y. Zhang, W. Shangguan, H. Yuan, S. Zhang, S. Liu and X. Lu (2019). "A global high-resolution data set of soil hydraulic and thermal properties for land surface modeling." Journal of Advances in Modeling Earth Systems **11**(9): 2996-3023.

de Araújo, J. C. and J. I. González Piedra (2009). "Comparative hydrology: analysis of a semiarid and a humid tropical watershed." Hydrological Processes: An International Journal **23**(8): 1169-1178.

Desborough, C. E. (1997). "The impact of root weighting on the response of transpiration to moisture stress in land surface schemes." Monthly Weather Review **125**(8): 1920-1930.

Didan, K. (2015). MOD13A3 MODIS/Terra vegetation indices monthly L3 global 1km SIN grid V006 (Data set) NASA EOSDIS Land Process, DAAC.

Feng, D., K. Fang and C. Shen (2020). "Enhancing streamflow forecast and extracting insights using long-short term memory networks with data integration at continental scales." Water Resources Research **56**(9): e2019WR026793.

Friedl, M. A., D. Sulla-Menashe, B. Tan, A. Schneider, N. Ramankutty, A. Sibley and X. Huang (2010). "MODIS Collection 5 global land cover: Algorithm refinements and characterization of new datasets." Remote sensing of Environment **114**(1): 168-182.

Gleeson, T., N. Moosdorf, J. Hartmann and L. Van Beek (2014). "A glimpse beneath earth's surface: GLobal HYdrogeology MaPS (GLHYMPS) of permeability and porosity." Geophysical Research Letters **41**(11): 3891-3898.

Gleeson, T., L. Smith, N. Moosdorf, J. Hartmann, H. H. Dürr, A. H. Manning, L. P. van Beek and A. M. Jellinek (2011). "Mapping permeability over the surface of the Earth." Geophysical Research Letters **38**(2).

Gudmundsson, L., M. Leonard, H. X. Do, S. Westra and S. I. Seneviratne (2019). "Observed trends in global indicators of mean and extreme streamflow." Geophysical Research Letters **46**(2): 756-766.

Hartmann, J. and N. Moosdorf (2012). "The new global lithological map database GLiM: A representation of rock properties at the Earth surface." Geochemistry, Geophysics, Geosystems **13**(12).

Hengl, T., J. Mendes de Jesus, G. B. Heuvelink, M. Ruiperez Gonzalez, M. Kilibarda, A. Blagotić, W. Shangguan, M. N. Wright, X. Geng and B. Bauer-Marschallinger (2017). "SoilGrids250m: Global gridded soil information based on machine learning." PLoS one **12**(2): e0169748.

Horn, B. K. (1981). "Hill shading and the reflectance map." Proceedings of the IEEE **69**(1): 14-47.

Huang, H., Y. Han, M. Cao, J. Song and H. Xiao (2016). "Spatial-temporal variation of aridity index of China during 1960–2013." Advances in Meteorology **2016**.

Knoben, W. J., J. E. Freer and R. A. Woods (2019). "Inherent benchmark or not? Comparing Nash–Sutcliffe and Kling–Gupta efficiency scores." Hydrology and Earth System Sciences **23**(10): 4323-4331.

Knyazikhin, Y. (1999). "MODIS leaf area index (LAI) and fraction of photosynthetically active radiation absorbed by vegetation (FPAR) product (MOD 15) algorithm theoretical basis document." http://eospso. gsfc. nasa. gov/atbd/modistabls. heml.

Kollat, J., P. Reed and T. Wagener (2012). "When are multiobjective calibration trade-offs in hydrologic models meaningful?" Water Resources Research **48**(3).

Kollat, J., P. Reed and T. J. W. R. R. Wagener (2012). "When are multiobjective calibration trade-offs in hydrologic models meaningful?" **48**(3).

Kratzert, F., D. Klotz, C. Brenner, K. Schulz and M. Herrnegger (2018). "Rainfall–runoff modelling using long short-term memory (LSTM) networks." Hydrology and Earth System Sciences **22**(11): 6005-6022.

Kratzert, F., D. Klotz, G. Shalev, G. Klambauer, S. Hochreiter and G. Nearing (2019). "Towards learning universal, regional, and local hydrological behaviors via machine learning applied to large-sample datasets." Hydrology & Earth System Sciences **23**(12).

Lane, R. A., G. Coxon, J. E. Freer, T. Wagener, P. J. Johnes, J. P. Bloomfield, S. Greene, C. J. Macleod and S. M. Reaney (2019). "Benchmarking the predictive capability of hydrological models for river flow and flood peak predictions across over 1000 catchments in Great Britain." Hydrology and Earth System Sciences **23**(10): 4011-4032.

LeCun, Y., Y. Bengio and G. J. n. Hinton (2015). "Deep learning." **521**(7553): 436-444.

Legasa, M. and J. M. Gutiérrez (2020). "Multisite Weather Generators using Bayesian Networks: An illustrative case study for precipitation occurrence." Water Resources Research **56**(7): e2019WR026416.

Lehner, B. (2014). HydroBASINS: Global watershed boundaries and sub-basin delineations derived from HydroSHEDS data at 15 second resolution—Technical documentation version 1. c.

Lehner, B., C. R. Liermann, C. Revenga, C. Vörösmarty, B. Fekete, P. Crouzet, P. Döll, M. Endejan, K. Frenken and J. J. T. D. Magome, Version (2011). "Global reservoir and dam (grand) database." **1**: 1-14.

Linke, S., B. Lehner, C. O. Dallaire, J. Ariwi, G. Grill, M. Anand, P. Beames, V. Burchard-Levine, S. Maxwell and H. Moidu (2019). "Global hydro-environmental sub-basin and river reach characteristics at high spatial resolution." Scientific data **6**(1): 1-15.

Liu, B., M. Xu, M. Henderson and W. Gong (2004). "A spatial analysis of pan evaporation trends in China, 1955–2000." Journal of Geophysical Research: Atmospheres **109**(D15).

Liu, Q., Z. Yang and X. Xia (2010). "Trends for pan evaporation during 1959-2000 in China." Procedia Environmental Sciences **2**: 1934-1941.

Liu, Y., J. Zheng, Z. Hao and X. Zhang (2017). "Unprecedented warming revealed from multi-proxy reconstruction of temperature in southern China for the past 160 years." Advances in Atmospheric Sciences **34**(8): 977-982.

Masutomi, Y., Y. Inui, K. Takahashi and Y. Matsuoka (2009). "Development of highly accurate global polygonal drainage basin data." Hydrological Processes: An International Journal **23**(4): 572-584.

Mei, Y., V. Maggioni, P. Houser, Y. Xue and T. Rouf (2020). "A nonparametric statistical technique for spatial downscaling of precipitation over High Mountain Asia." Water Resources Research **56**(11): e2020WR027472.

https://doi.org/10.5194/essd-2021-71
Preprint. Discussion started: 21 April 2021

Myneni, R., Y. Knyazikhin and T. Park (2015). "MOD15A2H MODIS/terra leaf area index/FPAR 8-day L4 global 500 m SIN grid V006." NASA EOSDIS Land Processes DAAC.

Nevo, S., V. Anisimov, G. Elidan, R. El-Yaniv, P. Giencke, Y. Gigi, A. Hassidim, Z. Moshe, M. Schlesinger and G. Shalev (2019). "ML for flood forecasting at scale." arXiv preprint arXiv:1901.09583.

Newman, A., M. Clark, K. Sampson, A. Wood, L. Hay, A. Bock, R. Viger, D. Blodgett, L. Brekke and J. Arnold (2015). "Development of a large-sample watershed-scale hydrometeorological data set for the contiguous USA: data set characteristics and assessment of regional variability in hydrologic model performance." Hydrology and Earth System Sciences **19**(1): 209-223.

Ni, H. and S. M. Benson (2020). "Using Unsupervised Machine Learning to Characterize Capillary Flow and Residual Trapping." Water Resources Research **56**(8): e2020WR027473.

Oudin, L., V. Andréassian, J. Lerat and C. Michel (2008). "Has land cover a significant impact on mean annual streamflow? An international assessment using 1508 catchments." Journal of hydrology **357**(3-4): 303-316.

Running, S., Q. Mu and M. Zhao (2017). MOD16A2 MODIS/Terra Net Evapotranspiration 8-Day L4 Global 500 m SIN Grid V006. NASA EOSDIS Land Processes DAAC.

Seybold, H., D. H. Rothman and J. W. Kirchner (2017). "Climate's watermark in the geometry of stream networks." Geophysical Research Letters **44**(5): 2272-2280.

Shangguan, W., Y. Dai, Q. Duan, B. Liu and H. Yuan (2014). "A global soil data set for earth system modeling." Journal of Advances in Modeling Earth Systems **6**(1): 249-263.

Shangguan, W., Y. Dai, B. Liu, A. Zhu, Q. Duan, L. Wu, D. Ji, A. Ye, H. Yuan and Q. Zhang (2013). "A China data set of soil properties for land surface modeling." Journal of Advances in Modeling Earth Systems **5**(2): 212-224.

Shen, C., E. Laloy, A. Elshorbagy, A. Albert, J. Bales, F.-J. Chang, S. Ganguly, K.-L. Hsu, D. Kifer and Z. Fang (2018). "HESS Opinions: Incubating deep-learning-powered hydrologic science advances as a community." Hydrology and Earth System Sciences (Online) **22**(11).

Silberstein, R. (2006). "Hydrological models are so good, do we still need data?" Environmental Modelling & Software **21**(9): 1340-1352.

Singh, R., S. Archfield and T. Wagener (2014). "Identifying dominant controls on hydrologic parameter transfer from gauged to ungauged catchments–A comparative hydrology approach." Journal of Hydrology **517**: 985-996.

Singh, R., K. van Werkhoven and T. Wagener (2014). "Hydrological impacts of climate change in gauged and ungauged watersheds of the Olifants basin: a trading-space-for-time approach." Hydrological Sciences Journal **59**(1): 29-55.

Subramanya, K. (2013). Engineering Hydrology, 4e, Tata McGraw-Hill Education.

Sulla-Menashe, D. and M. A. Friedl (2018). "User guide to collection 6 MODIS land cover (MCD12Q1 and MCD12C1) product." USGS: Reston, VA, USA: 1-18.

Survey, C. G. (2001). "1:2,500,000-scale digital geological map database of China."

Tyralis, H., G. Papacharalampous and S. Tantanee (2019). "How to explain and predict the shape parameter of the generalized extreme value distribution of streamflow extremes using a big dataset." Journal of Hydrology **574**: 628-645.

van Werkhoven, K., T. Wagener, P. Reed and Y. J. W. R. R. Tang (2008). "Characterization of watershed model behavior across a hydroclimatic gradient." **44**(1).

van Wijk, M. T. and M. Williams (2005). "Optical instruments for measuring leaf area index in low vegetation: application in arctic ecosystems." Ecological Applications **15**(4): 1462-1470.

Viglione, A., M. Borga, P. Balabanis and G. Blöschl (2010). "Barriers to the exchange of hydrometeorological data in Europe: Results from a survey and implications for data policy." Journal of Hydrology **394**(1-2): 63-77.

Voepel, H., B. Ruddell, R. Schumer, P. A. Troch, P. D. Brooks, A. Neal, M. Durcik and M. Sivapalan (2011). "Quantifying the role of climate and landscape characteristics on hydrologic partitioning and vegetation response." Water Resources Research **47**(10).

Wang, J., M. Chen, G. Lü, S. Yue, Y. Wen, Z. Lan and S. Zhang (2020). "A data sharing method in the open web environment: Data sharing in hydrology." Journal of Hydrology **587**: 124973.

Wickel, B., B. Lehner and N. Sindorf (2007). HydroSHEDS: A global comprehensive hydrographic dataset. AGU Fall Meeting Abstracts.

Wongso, E., R. Nateghi, B. Zaitchik, S. Quiring and R. Kumar (2020). "A Data-Driven Framework to Characterize State-Level Water Use in the United States." Water Resources Research **56**(9): e2019WR024894.

Woods, R. A. J. A. i. W. R. (2009). "Analytical model of seasonal climate impacts on snow hydrology: Continuous snowpacks." **32**(10): 1465-1481.

Xinjiang, B. o. G. a. M. R. o. (1992). "Geological map of Xinjiang Uygur, Autonomous Region, China, version 2, scale 1:1,500,000."

Xu, Y., X. Gao, Y. Shen, C. Xu, Y. Shi and a. Giorgi (2009). "A daily temperature dataset over China and its application in validating a RCM simulation." Advances in Atmospheric sciences **26**(4): 763-772.

Yamazaki, D., D. Ikeshima, J. Sosa, P. D. Bates, G. H. Allen and T. M. Pavelsky (2019). "MERIT Hydro: a high-resolution global hydrography map based on latest topography dataset." Water Resources Research **55**(6): 5053-5073.

Zeng, X. (2001). "Global vegetation root distribution for land modeling." Journal of Hydrometeorology **2**(5): 525-530.